



IRON-GROUP ABUNDANCES IN THE METAL-POOR MAIN-SEQUENCE TURNOFF STAR HD 84937

CHRISTOPHER SNEDEN¹, JOHN J. COWAN², CHIAKI KOBAYASHI³, MARCO PIGNATARI^{4,6}, JAMES E. LAWLER⁵, ELIZABETH A. DEN HARTOG⁵, AND MICHAEL P. WOOD^{5,7}¹ Department of Astronomy and McDonald Observatory, The University of Texas, Austin, TX 78712, USA; chris@verdi.as.utexas.edu² Homer L. Dodge Department of Physics and Astronomy, University of Oklahoma, Norman, OK 73019, USA; jjcowan1@ou.edu³ School of Physics, Astronomy and Mathematics, Centre for Astrophysics Research, University of Hertfordshire, College Lane, Hatfield AL10 9AB, UK; c.kobayashi@herts.ac.uk⁴ Konkoly Observatory, Research Centre for Astronomy and Earth Sciences, Hungarian Academy of Sciences, Konkoly Thege Miklos ut 15-17, H-1121 Budapest, Hungary⁵ Department of Physics, University of Wisconsin-Madison, 1150 University Ave., Madison, WI 53706, USA; jelawler@wisc.edu, eadenhar@wisc.edu, michael.wood@nist.gov

Received 2015 August 17; accepted 2015 October 28; published 2016 January 20

ABSTRACT

We have derived new, very accurate abundances of the Fe-group elements Sc through Zn ($Z = 21 - 30$) in the bright main-sequence turnoff star HD 84937 based on high-resolution spectra covering the visible and ultraviolet spectral regions. New or recent laboratory transition data for 14 species of seven elements have been used. Abundances from more than 600 lines of non-Fe species have been combined with about 550 Fe lines in HD 84937 to yield abundance ratios of high precision. The abundances have been determined from both neutral and ionized transitions, which generally are in agreement with each other. We find no substantial departures from the standard LTE Saha ionization balance in this $[\text{Fe}/\text{H}] = -2.32$ star. Noteworthy among the abundances are $[\text{Co}/\text{Fe}] = +0.14$ and $[\text{Cu}/\text{Fe}] = -0.83$, in agreement with past studies of abundance trends in this and other low-metallicity stars, and $\langle [\text{Sc}, \text{Ti}, \text{V}/\text{Fe}] \rangle = +0.31$, which has not been noted previously. A detailed examination of scandium, titanium, and vanadium abundances in large-sample spectroscopic surveys reveals that they are positively correlated in stars with $[\text{Fe}/\text{H}] < -2$; HD 84937 lies at the high end of this correlation. These trends constrain the synthesis mechanisms of Fe-group elements. We also examine the Galactic chemical evolution abundance trends of the Fe-group elements, including a new nucleosynthesis model with jet-like explosion effects.

Key words: atomic data – Galaxy: evolution – nuclear reactions, nucleosynthesis, abundances – stars: abundances – stars: individual (HD 84937) – stars: Population II

Supporting material: machine-readable tables

1. INTRODUCTION

Massive stars began producing heavy elements near the birth of our Galaxy. The records of their nucleosynthesis contributions are written into the chemical compositions of very metal-poor stars of the Galactic halo. If accurate abundances can be extracted for whole element groups in these low-metallicity stars, it will be possible to better understand their nucleosynthetic messages.

Over the past 15 years there have been major advances in our understanding of the abundances of neutron-capture elements (n -capture, $Z > 30$) in metal-poor stars. Many of these stars have extremely detailed n -capture abundance distributions, with accurate abundances for more than 30 elements. We know that their bulk n -capture contents with respect to lighter elements vary by orders of magnitude from star to star (e.g., Sneden et al. 2008 and references therein). Moreover, their nucleosynthetic origin in a given star can be attributed to rapid neutron captures (the r -process; Thielemann et al. 2011 and references therein), or slow neutron captures (the s -process; Käppeler et al. 2011 and references therein), or a variety of other processes that can contribute to the zoo of anomalous abundances observed in old halo stars (e.g., Cowan & Rose 1977; Travaglio et al. 2004; Fröhlich et al. 2006b; Wanajo et al. 2006; Pignatari et al. 2008; Farouqi et al. 2010;

Arcones & Montes 2011; Herwig et al. 2011). A major reason for these insights has been the rapid increase in reliability of basic atomic transition data for the n -capture elements (e.g., Lawler et al. 2009; Sneden et al. 2009 and references therein). As the transition probabilities, isotopic splittings, and hyperfine structures have become more reliable, the derived n -capture abundances have also become more accurate.

The same generally cannot be said for lighter elements, in particular for the Fe-group ($21 \leq Z \leq 30$). There have been many large-sample spectroscopic surveys of Fe-group elements in halo stars beginning more than 30 years ago, with the spectroscopic quality increasing with time. The pioneering surveys of Luck & Bond (1985) and McWilliam et al. (1995) have been followed by more detailed studies by, e.g., those of Cayrel et al. (2004), Barklem et al. (2005), Yong et al. (2013), and Roederer et al. (2014) for red giants, and that of Cohen et al. (2004) for main-sequence stars. But the reliability of the reported abundances in any of these surveys is not assured. First, for many stars, not all Fe-group elements are detectable with the available spectra. Second, even when elements can be detected, often only neutral-species transitions are available for analysis in typical ground-based spectra. The ionization balances of Fe-group elements in metal-poor warmer dwarfs and cooler red giants usually are dominated by the ionized species; therefore the elemental abundances are mostly based on results from the minority species. Third, in many instances only a handful of lines are employed to form individual elemental abundances. Finally, significant questions have been

⁶ NuGrid collaboration; <http://www.nugridstars.org>.

⁷ Current address: National Institute of Standards and Technology, Gaithersburg, MD 20899, USA.

raised about whether local thermodynamic equilibrium (LTE) can adequately describe the ionization equilibrium, and large upward corrections have been proposed to LTE-based abundances from neutral species.

Our group has been concentrating on improving the laboratory data for Fe-group neutral and singly ionized transitions that are of interest to cool-star stellar spectroscopy. Citations to individual papers within this series will be given in Section 3. In each study we have used the new atomic data to rederive abundances in the solar photosphere and in the very metal-poor ($[\text{Fe}/\text{H}] \sim -2.2^8$) main-sequence turnoff star HD 84937. This star has been chosen because of its brightness, well-known atmospheric parameters, and availability of good high-resolution spectra over a very large wavelength range. In this paper we will finish our reconnaissance of the Fe-group elements in HD 84937.

In Section 2 we introduce the high-resolution spectroscopic data sets analyzed for the solar photosphere and HD 84937. New abundances of several elements and summaries of recent results for other elements are given in Section 3. Interpretation and discussion of the iron-peak data and abundances, particularly nucleosynthesis origins and production mechanisms, are included in Section 4. The implications for Galactic chemical evolution (GCE), accompanied by detailed models, follow in Section 5. Finally, a summary and conclusions are detailed in Section 6.

2. SPECTROSCOPIC DATA AND ANALYSES

Solar and HD 84937 data sets are the same as in previous papers of this series. The spectra have been discussed in detail by Lawler et al. (2013); here we provide a brief summary. For the Sun we used the photospheric center-of-disk spectrum of Delbouille et al. (1973).⁹ The ground-based spectrum of HD 84937 was obtained from the ESO Very Large Telescope UVES archive.¹⁰ It extends over $3100 \lesssim \lambda \lesssim 10000 \text{ \AA}$, with resolving power $R \equiv \lambda/\Delta\lambda \sim 60,000$ and signal-to-noise ratio $S/N \sim 100$ at 3500 \AA , increasing steadily at longer wavelengths to a maximum $S/N \sim 300$. The vacuum-UV spectrum of HD 84937 comes from the *Hubble Space Telescope* Imaging Spectrograph (*HST*/STIS) public archive, having been part of proposal #7402 (PI: R. C. Peterson) and originally used in a study of chromospheric emission in metal-poor main-sequence stars (Peterson & Schrijver 1997). For this observation, *HST*/STIS used its E230M grating to produce a wavelength range $2280 \lesssim \lambda \lesssim 3120 \text{ \AA}$, $R \sim 25,000$, and average $S/N \sim 50$ after coaddition of the two spectra obtained for this star.

The adopted model solar photosphere is the empirical one determined by Holweger & Müller (1974), hereafter called **HM**. This model was used in the first of our atomic transition papers (Lawler et al. 2001), and we have stayed with this choice for all succeeding papers to maintain internal consistency. Likewise, for HD 84937 we again employ an interpolated model from the Kurucz (2011)¹¹ database, using adopted parameters $T_{\text{eff}} = 6300 \text{ K}$, $\log g = 4.0$, $\xi_t = 1.5 \text{ km s}^{-1}$,

and $[\text{Fe}/\text{H}] = -2.15$. A detailed discussion of these parameter choices can be found in Lawler et al. (2013), but a few points should be highlighted. First, since HD 84937 is a nearby ($d = 73 \pm 3 \text{ pc}$), warm ($B - V = 0.36$) main-sequence turnoff star, its T_{eff} and $\log g$ can be very well determined from parallax and photometry alone, without reference to spectroscopic constraints. Second, HD 84937 has been analyzed repeatedly for estimation of its $^6\text{Li}/^7\text{Li}$ ratio (Lind et al. 2013 and references therein), so its atmospheric parameters have been determined many times. A list of past analyses can be found in the SAGA database (Suda et al. 2008)¹²; all of these studies derive similar atmospheric parameters. Third, the relatively high temperature and gravity of HD 84937 combine to produce large densities that favor LTE approximations for atomic-level populations and Planck source functions; such simplifications are much more problematic for cool, metal-poor red giants. Finally, the same atmospheric conditions lead to continuum opacities that are dominated by H^- at most wavelengths; continuum scattering is unimportant even in the UV spectral region.

Abundances were derived following the methods of our previous papers. We computed synthetic spectra in small spectral intervals surrounding all photospheric transitions with the current version of the LTE line analysis code MOOG¹³ (Sneden 1973). Atomic and molecular line lists for the syntheses were based on the transitions compiled in the Kurucz (2011) database.¹⁴ These lists were updated with (a) new Fe-group transition probabilities and isotopic/hyperfine substructures presented in this series of papers; (b) similar data from our earlier publications on n -capture elements (Sneden et al. 2009 and references therein); and (c) recent molecular laboratory data on C_2 (Brooke et al. 2013; Ram et al. 2014), CH (Masseron et al. 2014), CN (Brooke et al. 2014; Sneden et al. 2014), and MgH (GharibNezhad et al. 2013; Hinkle et al. 2013). The computed solar spectra were smoothed with Gaussians to account for the instrument profile and solar macroturbulence and then compared to the center-of-disk solar spectrum of Delbouille et al. (1973) to estimate the line-by-line abundances. This procedure was also followed for HD 84937, except that here we used the version of MOOG that has scattering included in the continuum source function (Sobeck et al. 2011). As pointed out in earlier papers, for this and other main-sequence turnoff stars the scattering contributions are not important. H^- dominates the continuum opacity, followed by H I in the Balmer continuum region ($3100\text{--}3650 \text{ \AA}$). Therefore we would have obtained essentially the same HD 84937 abundances with the standard MOOG version.

3. NEW AND RECENT FE-GROUP SOLAR AND HD 84937 ABUNDANCES

In this section we discuss our analyses of the solar photosphere and HD 84937. Table 1 contains the abundances, standard deviations, and numbers of transitions for neutral and singly ionized (hereafter, “ionized”) species of these elements.

In Table 2 we compare our “new” solar abundances to the recent detailed analyses of Scott et al. (2015) for Sc–Ni, and of Grevesse et al. (2015) for Cu and Zn. Also tabulated are solar photospheric abundances recommended in the review by

⁸ We adopt the standard spectroscopic notation (Wallerstein & Helfer 1959) that for elements A and B, $[\text{A}/\text{B}] \equiv \log_{10}(N_{\text{A}}/N_{\text{B}})_{\star} - \log_{10}(N_{\text{A}}/N_{\text{B}})_{\odot}$. We use the definition $\log \epsilon(\text{A}) \equiv \log_{10}(N_{\text{A}}/N_{\text{H}}) + 12.0$ and equate metallicity with the stellar $[\text{Fe}/\text{H}]$ value.

⁹ Available at http://bass2000.obspm.fr/solar_spect.php

¹⁰ Under programs 073.D-0024 (PI: C. Akerman) and 266.D-5655 (Service Mode).

¹¹ <http://kurucz.harvard.edu/grids.html>

¹² Available at <http://saga.sci.hokudai.ac.jp/wiki/doku.php>

¹³ Available at <http://www.as.utexas.edu/~chris/moog.html>

¹⁴ Available at <http://kurucz.harvard.edu/linelists.html>

Table 1
Species Abundances

Element	log ϵ	σ	Num	log ϵ	σ	Num
	I	I	I	II	II	II
Solar Photosphere						
Sc	3.167 ± 0.014	0.056	15
Ti	4.973 ± 0.003	0.040	168	4.979 ± 0.005	0.054	43
V	3.956 ± 0.004	0.037	93	3.950 ± 0.010	0.050	15
Cr	5.650 ± 0.007	0.068	87	5.630 ± 0.030	0.153	13
Mn	5.451 ± 0.011	0.050	19	5.400 ± 0.000	0.000	1
Fe	7.522 ± 0.004	0.047	152	7.511 ± 0.021	0.082	16
Co	4.955 ± 0.007	0.059	82
Ni	6.277 ± 0.004	0.055	76
Cu	4.210 ± 0.013	0.033	7
Zn	4.610 ± 0.050	0.087	3
HD 84937						
Sc	1.081 ± 0.007	0.035	25
Ti	3.122 ± 0.007	0.054	54	3.081 ± 0.007	0.087	147
V	1.890 ± 0.030	0.070	9	1.871 ± 0.009	0.075	68
Cr	3.304 ± 0.018	0.098	31	3.437 ± 0.008	0.097	78
Mn	2.843 ± 0.019^a	0.083	19	2.881 ± 0.008	0.026	10
Fe	5.202 ± 0.003	0.069	446	5.193 ± 0.006	0.059	105
Co	2.787 ± 0.008	0.068	66	2.771 ± 0.020	0.079	15
Ni	3.888 ± 0.008	0.068	77	3.890 ± 0.040	0.100	8
Cu	$1.060 \pm (0.03)^b$	$(0.07)^b$	2
Zn	2.450 ± 0.037	0.075	4

Notes.

^a The mean abundance from Mn I lines has been computed with exclusion of the 4030, 4033, 4034 Å resonance triplet.

^b The Cu σ value has been assigned to more realistically represent its abundance uncertainty in HD 84937, and the mean abundance error follows from that and the number of lines.

Asplund et al. (2009) and the meteoritic abundances recommended by Lodders et al. (2009). We quote four values for each species from Scott et al. and Grevesse et al. Three of these abundances come from their papers, and the values that they obtained from their LTE analyses with the Holweger & Müller (1974) model solar photosphere are from P. Scott (2015, private communication). Our abundances are essentially identical to their LTE values; differences in detail can be attributed to line choices, transition probability assumptions, and so on. Scott et al. and Grevesse et al. consider in detail the various issues involved in photospheric abundance determinations, including choice of model atmosphere grid, one-dimensional (1D) versus three-dimensional (3D) atmospheric structure, and local versus nonlocal thermodynamic equilibrium (LTE versus NLTE) in atomic-level populations and line source functions. The reader is urged to consult those papers for additional information on solar abundance calculations and their uncertainties.

Our Fe-group abundances of HD 84937 have been determined from a total of 1162 spectral features (551 lines of neutral and ionized Fe and 611 of other elements). The number of lines used for each species is depicted in Figure 1. Only Cu and Zn abundances have been determined from a single species with less than five lines each. For Sc, only the ionized lines are detectable, but 25 of these form the elemental mean abundance.

Eight elements in this study have abundances determined from ionized transitions, with no fewer than eight lines forming the means of each species abundance. This is important because ions comprise the vast majority of the total numbers for all Fe-group elements except Zn. We illustrate this point in Figure 2 with number-density ratios $\log(N_{\text{ion}}/N_{\text{neutral}})$ plotted

as functions of optical depth, from straightforward Saha equation calculations. Five of the elements are completely ionized, defined here as $\log(N_{\text{ion}}/N_{\text{neutral}}) \gtrsim 2$, throughout the HD 84937 atmosphere. Four other elements have $\log(N_{\text{ion}}/N_{\text{neutral}}) \gtrsim 1.3$, meaning that the ionized species are at least 20 times more abundant than the neutral species at all atmospheric levels. The sole exception is Zn, whose ionization potential of 9.39 eV is high enough to keep a substantial fraction in its neutral species.

Our analyses of Ti, V, Co, and Ni have been discussed in detail in previous papers of this series, and those results will be summarized together in Section 3.2. We have comparatively little information on Cu and Zn, and none of their laboratory data have been generated in this series of papers; thus we will deal briefly with them together in Section 3.6. The remaining elements Sc, Cr, Mn, and Fe have transition data published by the University of Wisconsin laboratory group and collaborators, but we have not applied these lab results previously to HD 84937. Each of the elements will be described in subsections below, beginning with the fundamental metallicity indicator Fe.

3.1. Iron

Neutral and ionized Fe lines are ubiquitous in the spectra of cool stars, and this element is almost always used as a surrogate for overall metallicity. It is unfortunate that Fe I and Fe II have not enjoyed comprehensive laboratory transition data studies in recent years. However, new accurate *gf* values for Fe I lines arising from excited states ($\chi_{\text{lower}} = 2.4\text{--}5.1$ eV) have been published by Den Hartog et al. (2014) and Ruffoni et al. (2014). If we combine these transition probabilities and those

Table 2
Solar $\log \epsilon$ Abundance Comparisons

Element	New ^a	Sc015 ^b HMLTE	Sc015 ^c HMNLTE	Sc015 ^d <3D>	Sc015 ^e rec	Asp09 ^f	Lod09 ^g
Neutral Species							
Sc	...	3.12	3.28	3.21	3.16	3.15	3.07
Ti	4.97	4.96	4.99	4.94	4.93	4.95	4.93
V	3.96	3.97	4.07	3.98	3.89	3.93	3.98
Cr	5.65	5.65	5.66	5.62	5.62	5.64	5.66
Mn	5.45	5.43	5.47	5.43	5.42	5.43	5.50
Fe	7.52	7.51	7.52	7.46	7.47	7.50	7.47
Co	4.96	4.94	4.99	4.96	4.93	4.99	4.89
Ni	6.28	6.24	6.24	6.20	6.20	6.22	6.22
Cu	4.21	4.22	4.21	4.16	4.18	4.19	4.27
Zn	4.61	4.55	4.53	4.52	4.56	4.56	4.65
Ionized Species							
Sc	3.19	3.20	3.19	3.17	3.16	3.15	3.07
Ti	4.97	4.97	4.97	4.97	4.93	4.95	4.93
V	...	4.03	4.03	...	3.89	3.93	3.98
Cr	5.63	5.63	5.63	5.65	5.62	5.64	5.66
Mn	5.42	5.43	5.50
Fe	7.46	7.46	7.46	7.51	7.47	7.50	7.47
Co	4.93	4.99	4.89
Ni	...	6.24	6.24	6.23	6.20	6.22	6.22
Cu	4.18	4.19	4.27
Zn	4.56	4.56	4.65

Notes.

^a New: this study.

^b Sc015: Scott et al. (2015) for Sc–Ni, Grevesse et al. (2015) for Cu, Zn; HMLTE: Holweger & Müller (1974) model, LTE; these values are from P. Scott (2015, private communication).

^c Sc015, HMNLTE: Holweger & Müller model, NLTE corrections.

^d Sc015, <3D>: three-dimensional model atmosphere with NLTE corrections.

^e Sc015, rec: final recommended photospheric value from both species.

^f Asp09: recommended photospheric value from Asplund et al. (2009).

^g Lod09: recommended meteoritic value from Lodders et al. (2009).

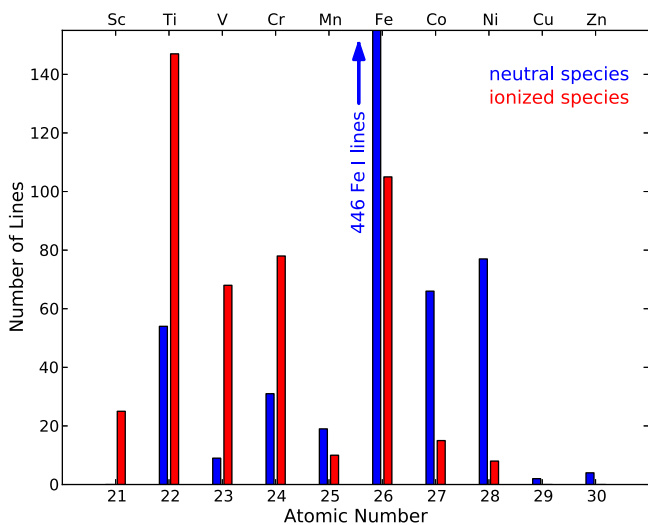


Figure 1. Number of measured transitions for neutral species (blue bars) and ionized species (red bars) in HD 84937. For display purposes, the vertical extent has been truncated at 150 lines, with an arrow indicating that there are far more Fe I lines than for other species. Single bars for Sc, Cu, and Zn indicate that only abundance results from Sc II, Cu I, and Zn I are available.

for lines with $\chi_{\text{lower}} < 2.4$ eV from the earlier study by O’Brian et al. (1991), a total of nearly 1100 Fe I lines from one collaborative laboratory research group can be applied to stellar spectra. This combined Fe I list should be on an internally consistent gf scale, and it has been adopted here.

We first applied the Fe I line list to the solar spectrum, but restricted the wavelength range to $4500 \text{ \AA} < \lambda < 6450 \text{ \AA}$. The blue limit was set by the steady increases in average Fe I line strengths and spectroscopic complexity due to other atomic and molecular species. The number of usable solar features drops precipitously below 4500 \AA . The red limit was set by the long-wavelength end of our Fe II line list (to be discussed below); thus the solar Fe abundance derived here depends on neutral and ionized lines arising in similar spectral regions. In Table 3 we list wavelengths, excitation energies, $\log gf$ values and their sources, and derived abundances for the Fe I lines used in the solar analysis, and in the upper panel of Figure 3 we display the photospheric line abundances as a function of wavelength. The scatter ($\sigma = 0.057$) is small and probably is limited by the solar analysis uncertainties. The mean abundance, $\log \epsilon = 7.523$ (Table 1), agrees with the Sc015 value derived with the HM model and is similar to other solar values (Table 2).

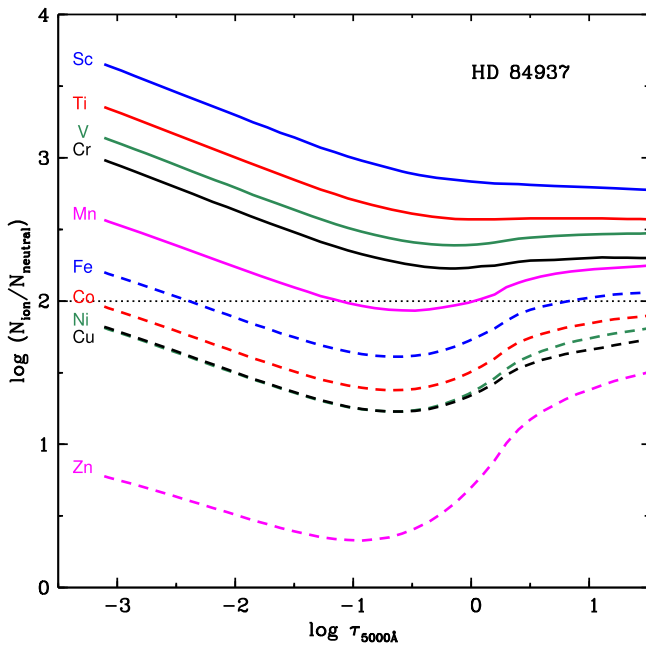


Figure 2. Logarithmic number density ionized-to-neutral species ratios of each Fe-group element as a function of optical depth at 5000 Å in the HD 84937 atmosphere. Element labels for the curves are written at the left in the figure. The dotted line at $\log(N_{\text{ion}}/N_{\text{neutral}}) = 2$ emphasizes the level at which the Saha ionization balance favors the ion by a factor of 100.

Table 3
Line Abundances for Fe I and Fe II

λ (Å)	Species	χ (eV)	$\log gf$	Source ^a	$\log \epsilon$ Sun	$\log \epsilon$ HD 84937
2297.79	Fe I	0.052	-1.10	Obr91	...	5.27
2298.66	Fe I	0.110	-2.42	Obr91	...	5.17
2299.22	Fe I	0.087	-1.55	Obr91	...	5.27
2309.00	Fe I	0.110	-1.39	Obr91	...	5.37
2369.46	Fe I	0.110	-2.19	Obr91	...	5.12
2371.43	Fe I	0.087	-1.95	Obr91	...	5.37
2374.52	Fe I	0.121	-2.10	Obr91	...	5.29
2389.97	Fe I	0.087	-1.57	Obr91	...	5.24
2438.18	Fe I	0.858	-1.25	Obr91	...	5.12
2453.48	Fe I	0.914	-0.92	Obr91	...	5.17

Note.

^a Den14: Den Hartog et al. (2014); Obr91: O’Brian et al. (1991); Ruf14: Ruffoni et al. (2014); NIST: NIST database.

(This table is available in its entirety in machine-readable form.)

There are no recent single-source lab transition studies of Fe II. Here we chose to use the gf values from the National Institute of Standards and Technology (NIST) Atomic Spectra Database¹⁵, which are based on a “critical compilation” (Fuhr & Wiese 2006) of previously published values. Since our transition probabilities are taken directly from the NIST website, we cite that source for the Fe II lines in Table 3. The original gf data are from (mostly experimental) papers by Bergeson et al. (1996), Raassen & Uylings (1998), Sikström et al. (1999), Donnelly & Hibbert (2001), Pickering et al. (2001, 2002), and Schnabel et al. (2004), which are cited for each line by NIST.

¹⁵ <http://physics.nist.gov/PhysRefData/ASD/>

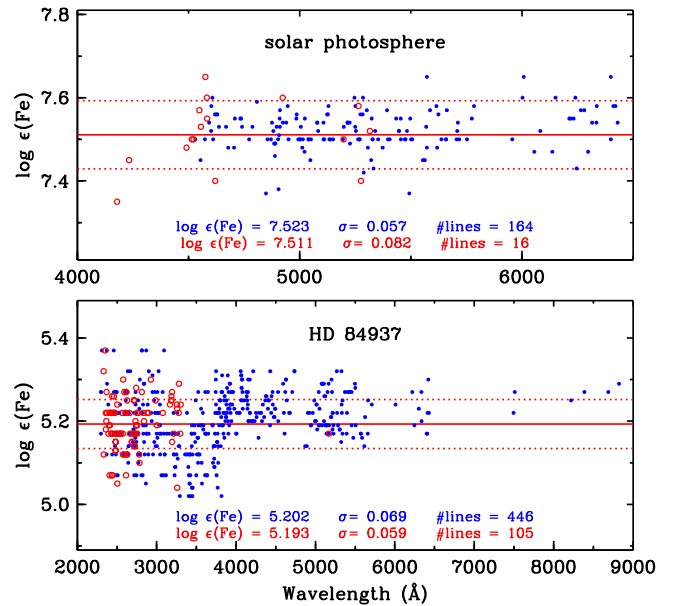


Figure 3. Abundances of Fe I and Fe II lines plotted as functions of wavelength for the solar photosphere (top panel) and HD 84937 (bottom panel). Blue symbols are for lines of the neutral species and red symbols for the ionized species. The species statistics from Table 1 are written at the bottom of each panel. A horizontal solid red line denotes the mean abundance from the ionized species, and the two dotted lines are displaced by $\pm\sigma$ from that mean. The vertical axis range in each panel is the ionized-species mean ± 0.3 dex. The horizontal axis range is chosen to be large enough to show all line abundances for the star and hence will be different for results from the solar photosphere and for HD 84937.

The number of available Fe II lines for a solar abundance analysis is not large, and in the end just 16 were used. We attempted to analyze only two Fe II lines with wavelengths below 4500 Å, deeming others to be too strong/weak/blended to yield reliable abundances. However, the mean abundance derived from Fe II lines is in agreement with the Fe I value. Recognizing the lack of comprehensive lab studies of Fe II, Meléndez & Barbuy (2009) combined some laboratory gf values with ones derived from a reverse solar analysis. However, the lower wavelength limit of their study was 4087 Å. Since our goal is to use as many lines as possible down to 2300 Å in the HD 84937 spectrum, we have not considered their data further here.

For HD 84937 we used the complete Fe I list and found 446 useful lines over the wavelength range $2300 \text{ \AA} \lesssim \lambda \lesssim 9000 \text{ \AA}$. These line abundances are given in Table 3 and plotted as a function of wavelength in the lower panel of Figure 3. This plot shows that the derived abundances have no trend with wavelength except for a dip in Fe abundances from lines in the Balmer continuum regions, an anomaly that was discussed extensively by Roederer et al. (2012) in a study of four metal-poor giants. The Fe I lines both blueward and redward of this region yield consistent abundances. We also derived Fe abundances for the Fe I lines using the transition probabilities from the Oxford (Blackwell et al. 1995 and references therein) and Hannover (Bard et al. 1991; Bard & Kock 1994) laboratory groups. For 61 lines in common with the Oxford group, $\langle \log(gf)_{\text{Oxford}} - \log(gf)_{\text{this study}} \rangle = -0.02$ with $\sigma = 0.09$. With these transition probabilities, the mean HD 84937 abundance for this line subset is 0.06 larger than than our value in Table 1. For 67 lines in common with the Hannover group, $\langle \log(gf)_{\text{Hannover}} - \log(gf)_{\text{this study}} \rangle = +0.02$ with $\sigma = 0.17$.

This large scatter is however caused entirely by disagreements between our preferred transition probabilities and theirs for vacuum-UV transitions. Excluding lines with $\lambda < 3000 \text{ \AA}$, the comparison is much more favorable: for the remaining 57 lines $(\log(gf)_{\text{Hannover}} - \log(gf)_{\text{this study}}) = 0.00$ with $\sigma = 0.05$, in agreement in derived Fe abundance with our value.

Many more Fe II lines are available in HD 84937 than in the solar photosphere. The line abundances (Table 3 and the lower panel of Figure 3) have no substantial trends with wavelength. The derived mean Fe abundances from both species are in agreement.

3.2. Titanium, Vanadium, Cobalt, and Nickel

Titanium: Our first studies of Fe-group transition data dealt with Ti I (Lawler et al. 2013) and Ti II (Wood et al. 2013). Large numbers of useful lines of both species are available in solar and HD 84937 spectra. The dominant Ti isotope is ^{48}Ti , comprising 73.7% of the total according to the KAERI database.¹⁶ The remaining 26.3% is spread fairly evenly among the $^{46,47,49,50}\text{Ti}$ isotopes. Fortunately, the isotopic splitting and hyperfine structures (hereafter, hfs) of odd-N isotopes $^{47,49}\text{Ti}$ are very narrow, producing negligible broadening of Ti emission lines in very high-resolution laboratory spectra. Therefore, Lawler et al. and Wood et al. treated the Ti transitions as single lines. We quote their results in Table 1. For the solar photosphere, the line-to-line scatter, $\sigma \lesssim 0.05$, is consistent with uncertainties in extracting abundances from matching observed and synthetic spectra.

For HD 84937, Lawler et al. (2013) noted a dip of ~ 0.2 dex in derived Ti I and Fe I abundances in the near-UV, $\lambda \sim 3100 - 3700 \text{ \AA}$. This abundance depression amounts to ~ 0.15 dex on average, about half that found by Roederer et al. (2012) in their four giant stars. Wood et al. (2013) found a similar anomaly for Ti II lines but mostly confined to those with excitation energies $\chi > 0.6 \text{ eV}$ (see their Figure 12). That paper's Section 8 discusses this issue, arguing that the abundance dip for HD 84937 is connected to the Balmer continuum opacity. For this warm main-sequence turnoff star, H^- dominates all opacity sources except in the $3100 - 3700 \text{ \AA}$ region, and the abundance dip is more mild than in cooler, lower gravity stars with weaker H^- opacity. Here we note that in Table 1 we have adopted the mean of all Ti II line abundances. If we were to neglect the $3100 - 3700 \text{ \AA}$ lines, the mean Ti abundance from this species would rise to $\log \epsilon \simeq 3.12$, in better agreement with the value derived from the Ti I lines. For our purposes this is not a concern, but future studies with a more comprehensive physical analysis will be welcome.

Vanadium: We presented new laboratory transition data for V I in Lawler et al. (2014) and for V II in Wood et al. (2014a). Vanadium's sole naturally occurring isotope is ^{51}V . Substantial hfs broadening is present in spectral features of both V I and V II. Laboratory hfs data are available for the majority of astronomically relevant transitions, and they were taken into account when possible (Lawler et al., Table 5, Figure 6; Wood et al., Table 5, Figure 4); see those papers for detailed hfs discussions. Good agreement was found between our solar abundances from both V species and the recommended photospheric and meteoritic values (Table 2). The Sc_{15} results for V I are about 0.05 dex smaller, and V II was not

considered by those authors. In HD 84937 the V I lines are all extremely weak, and the dominant analytical problem becomes one of detection (Lawler et al., Figure 7). Nonetheless, satisfactory abundance agreement was achieved between the two V species in this star.

Cobalt: A new lab/stellar study of Co I has been completed by Lawler et al. (2015). This element's only naturally occurring isotope is ^{59}Co , and most Co I transitions have significant hfs. For the solar photosphere, synthetic spectrum computations for 82 lines, most of which have hfs components included in the computations, yielded the mean abundance quoted in Table 1. There are 23 lines of Co II identified by Moore et al. (1966) in the $3300 - 4700 \text{ \AA}$ spectral range, but these lines have not had recent transition probability analyses. The NIST database gives poor grades to their gf values, so Lawler et al. (2015) did not investigate this species in the Sun. Application of the new Co I lab data to the HD 84937 spectrum led to the abundance given in Table 1. Fortunately, the *HST*/STIS spectrum contains lines of Co II with more reliable transition probabilities. A total of 15 lines of this species yielded a mean abundance that is in excellent agreement with that obtained from Co I.

Nickel: Wood et al. (2014b) reported new transition probabilities for Ni I. While Ni lines have negligible hfs, in the red spectral region the isotopic splitting among its five naturally occurring isotopes (^{58}Ni , 68.1%, KAERI database; ^{60}Ni , 26.2%; ^{61}Ni , 1.1%; ^{62}Ni , 3.6%; and ^{64}Ni , 0.9%) is detectable in the solar spectrum. Wood et al. included isotopic substructure when possible in their calculations. For the solar photosphere their derived abundance was about 0.06 dex larger than other values from the literature (Table 2; see Wood et al.), but within the mutual uncertainties of their and other values. Transitions of Ni II have been identified in the solar spectrum (Moore et al. 1966), but they arise from excited-state lower levels ($\chi \gtrsim 3 \text{ eV}$), and their transition probabilities have not been studied in the lab for about three decades. Lines of Ni I redward of 5000 \AA are numerous in the solar spectrum but are mostly undetectable in HD 84937. But many transitions of this species at shorter wavelengths are available for analysis in this very metal-poor star. Moreover, strong lines of Ni II from lower excitation levels ($\chi = 1.0 - 2.0 \text{ eV}$) with more recent lab gf values (Fedchak & Lawler 1999) can be found in the vacuum-UV spectral range. In Table 1 we quote the Wood et al. abundances from both Ni species in HD 84937, which clearly are in agreement.

3.3. Scandium

For this paper we only consider Sc II transitions. All useful solar Sc I lines are very weak. In the photospheric abundance studies of Neuforge (1993, pp. 63–65) and Sc_{15} , the strongest line of this species is at 5671.8 \AA , with $\text{EW} \simeq 12 \text{ m\AA}$, or $\log \text{RW} \equiv \log(\text{EW}/\lambda) \simeq -5.7$. Most other useful solar lines of this species are much weaker. The low metallicity of HD 84937 combined with its very large atmospheric $N_{\text{Sc II}}/N_{\text{Sc I}}$ ratio (Figure 2) conspire to make its Sc I lines undetectable.

The most recent laboratory transition probabilities are from Lawler & Dakin (1989), and they are adopted here for all Sc II transitions. When possible we included hfs in the abundance calculations. We calculated the hfs patterns from hyperfine constants given in Arnesen et al. (1982), Young et al. (1988), Mansour et al. (1989a, 1989b), and Villemoes et al. (1992).

¹⁶ Chang, J.: Table of Nuclides, Korea Atomic Energy Research Institute (KAERI); available at: <http://atom.kaeri.re.kr/ton/>

Table 4
Line Abundances for Other Fe-group Species

λ (Å)	Species	χ (eV)	$\log gf$	Source ^a	$\log \epsilon$ Sun	$\log \epsilon$ HD 84937
2552.35	Sc II	0.022	0.03	Law89	...	1.00
2563.19	Sc II	0.000	-0.58	Law89	...	1.05
3353.72	Sc II	0.315	0.25	Law89	...	1.07
3359.68	Sc II	0.008	-0.74	Law89	...	1.10
3368.93	Sc II	0.008	-0.37	Law89	...	1.07
3535.71	Sc II	0.315	-0.47	Law89	...	1.05
3567.69	Sc II	0.000	-0.48	Law89	...	1.06
3576.34	Sc II	0.008	0.01	Law89	...	1.04
3580.92	Sc II	0.000	-0.15	Law89	...	1.08
3589.63	Sc II	0.008	-0.57	Law89	...	1.09

Note.

^a Law89: Lawler & Dakin (1989); Sob07: Sobek et al. (2007); Gur10: Gurell et al. (2010); Nil06: Nilsson et al. (2006); Den11: Den Hartog et al. (2011); NIST: NIST database; Roe14: Roederer et al. (2014).
(This table is available in its entirety in machine-readable form.)

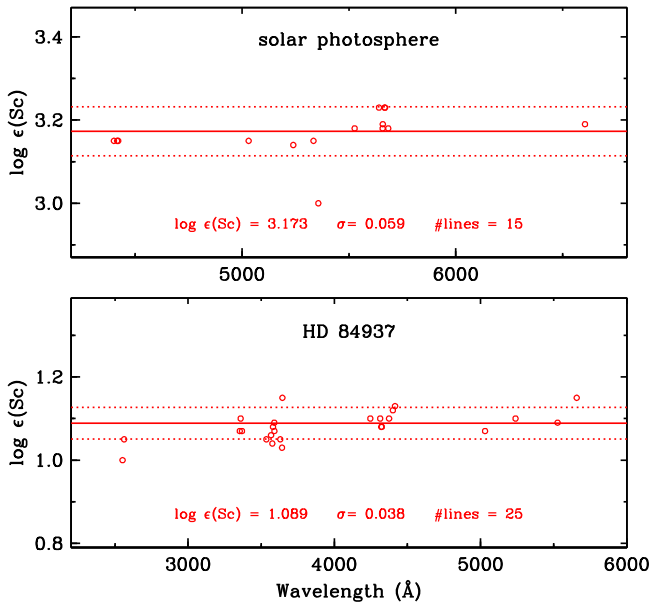


Figure 4. Abundances of Sc II lines plotted as functions of wavelength. All lines and points are as defined in Figure 3.

The majority of useful solar photospheric Sc II lines are in the yellow-red, and from 15 of them (Table 4) we derive a Sc abundance of $\log \epsilon = 3.17$ (Table 1 and Figure 4) that is in good agreement with other photospheric values (Table 2).¹⁷ The photospheric Sc abundance is about 0.1 dex higher than the meteoritic abundance recommended by Lodders et al. (2009), a discrepancy already noted by Sco15. Resolution of this discrepancy is beyond the scope of this work.

¹⁷ The five Sc II lines between 5600 and 5700 Å are part of the z^3P to a^3P multiplet. This multiplet is primarily responsible for the apparent Saha imbalance of Sc in the Sun (e.g., Neuforge 1993). Branching fraction measurements on this minor multiplet are challenging because of its large wavelength separation from the dominant UV branches of the z^3P upper levels and the absence of intermediate-wavelength lines. Remeasurement of Sc I and Sc II branching fractions is underway, and more than 90% of the Lawler & Dakin (1989) $\log(gf)$ values have been reproduced to within error bars. Preliminary evidence suggests that the $\log(gf)$ values of the z^3P to a^3P multiplet by Lawler & Dakin (1989) may be too small by about twice their ± 0.05 dex uncertainty.

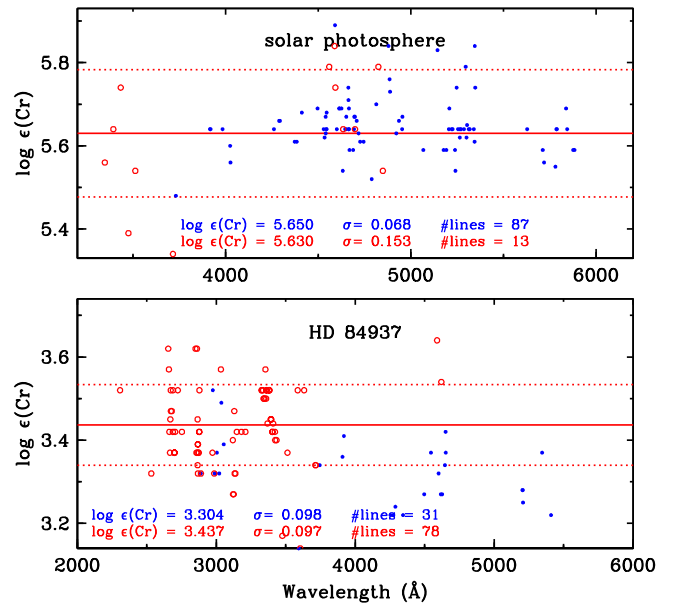


Figure 5. Abundances of Cr I and Cr II lines plotted as functions of wavelength. All lines and points are as defined in Figure 3.

More Sc II violet-UV transitions become available in the HD 84937 spectrum, and the 25 lines used in our analysis (Table 4) have excellent internal abundance agreement, with $\sigma = 0.038$ (Table 1 and Figure 4).

3.4. Chromium

This element has received recent attention from laboratory spectroscopists: Cr I by Sobek et al. (2007), and Cr II by Nilsson et al. (2006), Gurell et al. (2010), and Engström et al. (2014). Unfortunately this has not led to agreement in the abundances derived from the two species. McWilliam et al. (1995) discovered that abundances derived from lines of Cr I exhibit a steady decline in $[Cr/Fe]$ at metallicities $[Fe/H] \lesssim -2$, reaching $[Cr/Fe] \sim -0.5$ at $[Fe/H] \lesssim -3$. This trend has been confirmed and refined by subsequent surveys, e.g., Cayrel et al. (2004); see a summary in Figure 20 of Kobayashi et al. (2006). However, the less-frequent results from Cr II analyses find no obvious decline: $[Cr/Fe] \approx 0$ over the entire metallicity range $-3.4 \lesssim [Fe/H] \lesssim +0.4$ (as summarized by Kobayashi et al. 2006). Indeed, Roederer et al. (2014) suggest that Cr II lines yield Cr overabundances in low-metallicity stars: $[Cr/Fe] \approx +0.2$.

Cr has four naturally occurring isotopes: ^{50}Cr , 4.2%; ^{52}Cr , 83.8%; ^{53}Cr , 9.5%; and ^{54}Cr , 2.4% (KAERI database). Not only does ^{52}Cr dominate the elemental abundance, but isotope shifts are small. We inspected very high-resolution Cr emission-line lab spectra obtained with the National Solar Observatory (NSO) 1 m FTS (Brault 1976) and accessible in the NSO archive¹⁸ and found all line profiles to be narrow and symmetric. Therefore we ignored hfs and isotopic substructure in our abundance analyses.

The line abundances for Cr I and Cr II are listed in Table 4. There are many available transitions for both species in the Sun and HD 84937, but inspection of Figure 5 reveals that scatters in the Cr line abundances of the Sun and HD 84937 are larger than for other Fe-group elements. For the Sun, the abundance

¹⁸ Available at <http://diglib.nso.edu/>

means (Table 1) derived from neutral and ionized lines are in agreement. A handful of Cr I lines yield anomalously large abundances, but these do not stand out in plots of abundance versus excitation potential or line strength. Very low values for a couple of near-UV Cr II lines are mainly responsible for the large scatter ($\sigma=0.153$) in its mean abundance; neglecting these lines would bring the abundances of the two species into better agreement.

For HD 84937, again there is a large scatter in individual line abundances (Table 1, Figure 5), and the now-familiar offset between Cr I and Cr II appears. However, the abundance difference is not large, 0.13 dex, and is at the level seen for this metallicity regime in Figures 20 and 21 of Kobayashi et al. (2006). Note that three Cr I lines yield abundances about 0.2 dex less than the mean value for this species, but excluding them would not change the mean significantly. Scott et al. (2015) have questioned the accuracy of the Nilsson et al. (2006) Cr II transition probabilities for those lines involved in their solar-abundance determinations. To test whether the chosen transition probabilities for Cr II lines could be contributing to the large line-to-line scatter and the ionization mismatch with abundances derived from Cr I, we recalculated the Cr II abundances with the *gf* values posted to the Kurucz (2011) database prior to Nilsson et al. (2006). The mean HD 84937 abundance from Cr II decreased by 0.13 dex, canceling the ionization balance problem. However, the internal scatter for Cr II grew substantially to $\sigma=0.25$, an unacceptably large value. This issue should be explored in more detail as part of future Cr studies in metal-poor stars; renewed lab studies should be part of that effort.

3.5. Manganese

Relative deficiencies of Mn in low-metallicity stars have been known since the early days of high-resolution stellar spectroscopy. This anomaly was noted by Wallerstein et al. (1963), and many studies suggest that $[\text{Mn}/\text{Fe}] \lesssim -0.4$ for $[\text{Fe}/\text{H}] < -1$ (see Figure 22 of Kobayashi et al. 2006). Most of the Mn abundance analyses in the literature have employed only Mn I lines. This is risky because Mn is almost completely ionized in HD 84937 (Figure 2) and in the Sun as well.

Laboratory investigations of Mn I and Mn II have been published by Den Hartog et al. (2011). Here we adopt their *gf* values and hfs patterns exclusively, so all of the transition data come from a single source. The solar photospheric Mn abundance derived from Mn I lines appears to be trustworthy. The line-to-line scatter is small (Table 4, Figure 6, upper panel), and the mean abundance agrees with other solar abundance estimates within mutual uncertainties (Table 2). We searched for suitable solar Mn II lines from the Den Hartog et al. list but found only one, 3497.5 Å. Unfortunately, that transition is part of a clump of other Fe-group lines. We were only able to derive an approximate abundance, $\log \epsilon \simeq 5.4$, for this line. It is consistent with the abundance derived from Mn I lines, but it should be viewed with caution. We have chosen not to quote this unreliable estimate in Table 1, and it is not considered further in the paper.

For HD 84937 there is significant scatter among the Mn I line abundances (Table 4, Figure 6, lower panel). In particular, the 4030, 4033, 4034 Å resonance triplet abundances are ~ 0.3 dex lower than the means of other Mn neutral and ionized species lines. We suggest that this is further evidence for departures from LTE in Mn I line formation involving ground-state lines.

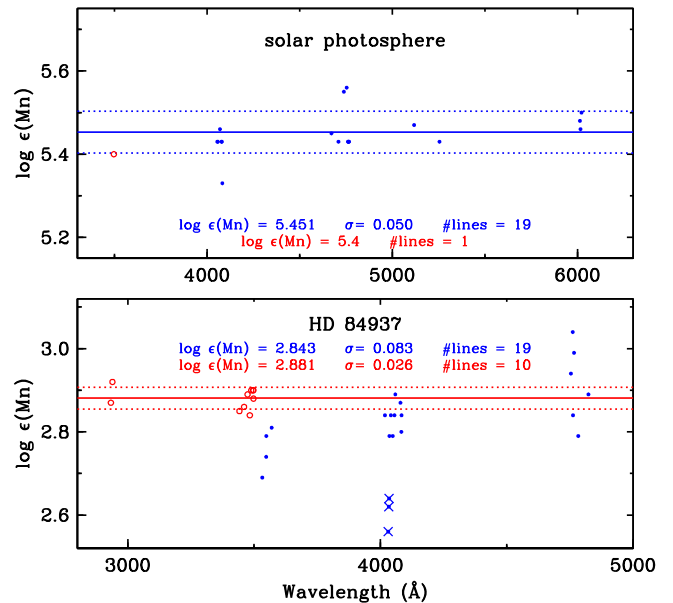


Figure 6. Abundances of Mn I and Mn II lines plotted as functions of wavelength. Most lines and points are as defined in Figure 3. In the top panel, we use blue horizontal lines to indicate that the mean and standard deviations are from Mn I because there is only one Mn II abundance point, and it is not very well determined. In the lower panel we use \times symbols to denote the abundances derived for the Mn I resonance triplet. Their abundances are depressed relative to other Mn I transitions, and hence they are not included in the abundance statistics.

Bergemann & Gehren (2008) computed such NLTE correction factors (see their Table 2) and found values to range from $\simeq 0.0$ dex at solar metallicity to as much as $\simeq 0.7$ dex at $[\text{Fe}/\text{H}] = -3$. In the $T_{\text{eff}}/\log g/[\text{Fe}/\text{H}]$ domain of HD 84937, the proposed NLTE corrections for Mn I lines are typically $\simeq 0.3$ – 0.4 dex, but for the resonance triplet they are $\simeq 0.5$ – 0.6 dex. This differential correction would nearly erase the abundance mismatch we see in the triplet lines compared to the rest of this species. Independent computation of NLTE effects is beyond the scope of this paper. Therefore we have chosen to exclude the Mn I triplet lines from the species mean given in Table 1 and shown in Figure 6. If we include the resonance triplet in the Mn I abundance statistics, the change would be small: $\langle \log \epsilon \rangle = 2.811 \pm 0.024$. The mean Mn abundance derived from Mn II lines in HD 84937 (Table 1) is only 0.04 dex larger than that derived from Mn I without the triplet.

3.6. Copper and Zinc

Copper and zinc present only a small number of detectable transitions of their neutral species in the spectra of the Sun and HD 84937. Strong lines of their first ions occur only in the deep UV spectral region, shortward of 2300 Å. We thus were unable to assess ionization equilibrium for either of these elements.

Both hyperfine and isotopic effects split Cu I lines into multiple components. There are two stable isotopes: ^{63}Cu , 69.2%, and ^{65}Cu , 30.8% (KAERI database). We adopted these percentages for the solar photosphere and, lacking isotopic information, for HD 84937. The hyperfine components were adopted from the Kurucz (2011) database. Accurate transition probabilities are known for the lines of interest here, and we adopted the values given in the NIST database. For the Sun, line-to-line agreement is excellent, and the mean Cu abundance is consistent with the Sco15 LTE value computed with the

Holweger & Müller (1974) atmosphere and with the Asplund et al. (2009) recommended photospheric abundance. Only the two Cu I resonance lines at 3247.5 and 3274.0 Å could be detected in our HD 84937 spectra, and they yield Cu abundances in fortuitously perfect agreement (Table 4). Here we have arbitrarily assigned an uncertainty $\sigma = 0.07$, a typical value for the other abundances in HD 84937.

Zinc is the only Fe-group element with a substantial population in the neutral species (Figure 2). Its detectable transitions in our spectra arise from excited lower-energy states, $\chi = 4.0$ eV. Both Saha and Boltzmann factors matter in the Zn I-level populations. We were able to derive mean Zn abundances from three lines in the solar photosphere and four lines in HD 84937. The line-to-line scatters are acceptable, and in the case of the Sun our derived abundance of $\log \epsilon(\text{Zn}) = 4.61$ splits the difference between other photospheric ($\simeq 4.55$) and meteoritic (4.65) values (Table 2). However, for HD 84937 our abundance is not as well constrained as those of other Fe-group elements, and it should be viewed with caution.

3.7. Abundance Uncertainties and Comments

Inspection of the HD 84937 abundances in Table 1 suggests that those derived from neutral and ionized species agree very well. In no case do the differences exceed their 1σ uncertainties. Thus we believe that, at least for seven of the 10 Fe-group elements, the Saha ionization balance is achieved with our standard spectroscopic analysis. Neutral species yield the same elemental abundances as the ionized species do. The derived abundances are the result of real nucleosynthesis output, not just stellar atmospheric effects.

This result holds with reasonable atmospheric parameter excursions from our baseline model of $T_{\text{eff}} = 6300$ K, $\log g = 4.0$, $\xi_t = 1.5$ km s $^{-1}$, and $[\text{Fe}/\text{H}] = -2.15$. The scatter in these parameters reported in the literature for HD 84937 are $\sigma(T_{\text{eff}}) \simeq 80$ K, $\sigma(\log g) \simeq 0.15$, $\sigma([\text{M}/\text{H}]) \simeq 0.15$, and $\sigma(\xi_t) \simeq 0.1$ (from papers included in the SAGA database). We calculated abundances for representative lines of each species for different atmosphere models that go beyond these probable uncertainties. In general, Fe-group neutral-species transitions collectively respond in a common way to parameter changes, as do all of the Fe-group ions. For temperature changes $\Delta T_{\text{eff}} = \pm 150$ K, $\Delta(\log \epsilon(\text{X I})) \simeq \pm 0.16$, and $\Delta(\log \epsilon(\text{X II})) \simeq \pm 0.06$. The positive correlation with T_{eff} is due to H $^-$ continuum opacity changes, and the difference between neutrals and ions is due to their own Saha balances. For gravity changes $\Delta \log g = \pm 0.25$, $\Delta(\log \epsilon(\text{X I})) \simeq \mp 0.06$, and $\Delta(\log \epsilon(\text{X II})) \simeq \pm 0.04$; this is a direct Saha effect. For model metallicity changes $\Delta[\text{M}/\text{H}] = \pm 0.25$, $\Delta(\log \epsilon(\text{X I})) \simeq \pm 0.01$, and $\Delta(\log \epsilon(\text{X II})) \simeq \pm 0.01$. This essentially null sensitivity to metallicity is because the major electron donor for the continuum opacity is H itself; heavy elements are minor contributors. Finally, since HD 84937 is a weak-lined star, the microturbulent velocity sensitivity is not large. For $\Delta \xi_t = \pm 0.15$, if $\log \text{RW} \lesssim -5.5$, then $\Delta(\log \epsilon(\text{X})) \simeq 0.00$ for lines of either neutral or ionized species, and if $\log \text{RW} \lesssim -4.5$, then $\Delta(\log \epsilon(\text{X})) \simeq \mp 0.05$.

However, these abundance sensitivities are muted in relative-abundance ratios. In our discussion to follow, we will concentrate on relative abundances $[X/\text{Fe}]$. We will be comparing neutral to neutral and ion to ion, and in almost all cases $\Delta(\log \epsilon(\text{X I}/\text{Fe I}))$ and/or $\Delta(\log \epsilon(\text{X II}/\text{Fe II})) \lesssim \pm 0.02$.

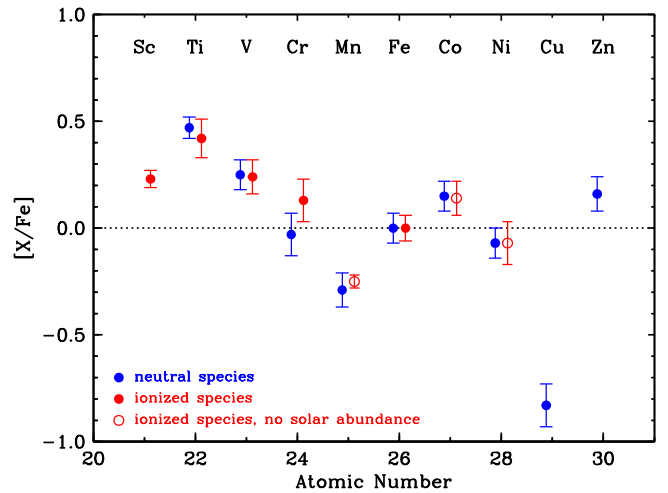


Figure 7. Abundance ratios in HD 84937 of all species with respect to Fe as a function of atomic number. For each element, neutral-species abundances are calculated with respect to the Fe I abundance and plotted in blue symbols offset to the left, and ions are calculated with respect to Fe II and are in red offset to the right. The error bars are $\pm 1\sigma$ values from Table 1.

Within our standard abundance analysis approach, model atmosphere parameter uncertainties cannot substantially perturb the abundances shown in Table 1.

Several cautions should be kept in mind in interpreting our results. (1) There are three “missing” species (Sc I, Cu II, Zn II) and three either with no solar abundance or an untrustworthy value (Mn II, Co II, Ni II). (2) Line formation in the Balmer continuum wavelength region is inadequately described by our standard modeling techniques. (3) Internal line-to-line scatters are large for Cr I and Cr II, and the agreement between the mean abundances for these two species is not as good as for the other Fe-group elements. (4) Mn I line-to-line scatter is large, and the resonance triplet yields abundances in HD 84937 that are nearly a factor of two lower than the mean of other neutral and ionized lines of this element. (5) Departures from LTE, not discussed in detail here, have been subjected to detailed calculations by others. In general, the neutral species appear to be much more sensitive to NLTE effects, leading to small predicted changes in derived solar abundances ($\lesssim 0.1$ dex, e.g., Grevesse et al. 2015 and references therein) but perhaps much larger corrections at low metallicities ($\lesssim 0.5$ dex, e.g., Lind et al. 2012 and references therein). Collectively, these issues clearly indicate the need for more laboratory effort, particularly for ionized species, and for more stellar atmosphere and line-formation modeling efforts. Our results have yielded promising results, but much further work in these areas will be welcome.

4. ABUNDANCE CORRELATIONS AMONG SC, TI, AND V IN HD 84937 AND OTHER LOW-METALLICITY STARS

In Figure 7 and Table 5 we present a summary of our results for the relative abundances of iron-group elements in HD 84937 using the traditional square-bracket units. Our compilation includes both neutral and ionized values where both are available. In Figure 7, abundances determined from neutral species with respect to Fe I are indicated by blue filled circles and from ionized species with respect to Fe II by red circles. As noted above, there are a few elements—denoted by open red circles—where no ionized solar values are available. In those cases, the solar ionization balance was assumed to determine the relative

Table 5
Final Relative Abundances in HD 84937

El	Z	[X/H]	σ	[X/H]	σ	[X/H]	[X/Fe]
		I	I	II	II	mean	mean
Sc	21	-2.09	0.04	-2.09	+0.23
Ti	22	-1.85	0.05	-1.90	0.09	-1.87	+0.45
V	23	-2.07	0.07	-2.08	0.08	-2.07	+0.25
Cr	24	-2.35	0.10	-2.19	0.10	-2.27	+0.05
Mn	25	-2.61	0.08	-2.57 ^a	0.03	-2.59	-0.27
Fe	26	-2.32	0.07	-2.32	0.06	-2.32	0.00
Co	27	-2.17	0.07	-2.18 ^a	0.08	-2.18	+0.14
Ni	28	-2.39	0.07	-2.39 ^a	0.10	-2.39	-0.07
Cu	29	-3.15	0.10	-3.15	-0.83
Zn	30	-2.16	0.08	-2.16	+0.16

Note.

^a No solar abundance is available from ionized-species lines. The [X/Fe] values have been computed using the derived solar abundance from neutral-species lines.

HD 84937 abundances, i.e., $\log \epsilon(X)_{\odot} \equiv \log \epsilon(X)_{\odot}$. It is clear from the figure that there is good agreement between the neutral and ionized species for the observed abundances in HD 84937. We also have listed overall mean relative abundances for these elements in Table 5, where we have averaged the neutral and ionized abundances (where available). The [X/Fe] values for HD 84937 in this table will be used in all further discussion in this paper.

It is also evident from Figure 7 that the abundances of the elements Sc, Ti, and V are enhanced with respect to solar values: their abundance ratios exceed the [X/Fe] = 0 horizontal dashed line in the figure. This result is not unique to HD 84937; it has been seen in other studies of low-metallicity stars (see, e.g., Yong et al. 2013; Roederer et al. 2014). We examine in Figure 8 the relationship between these abundances, first between the abundance ratios [Ti II/Fe II] and [V II/Fe II] from the extensive abundance data of Roederer et al. (2014). In panel (a) abundance ratios for stars with detectable Ti II and V II lines are shown along with the newly determined abundance values [Ti II/Fe II] and [V II/Fe II] for HD 84937 from this paper.¹⁹ Several trends are evident from this figure.

First, the majority of the observed data are above solar values; note the dashed lines indicating solar ratios. Caution is warranted here, and inclusion of upper limits would undoubtedly add to the count of stars with subsolar abundance ratios of these elements with respect to Fe. Second, while there is some abundance scatter, it is clear that the relative abundances of Ti and V are correlated. As a guide we have plotted a 45° (solid) line over the data. This line is consistent with the general trend of the Roederer et al. (2014) data and intersects the abundance values for HD 84937.

An additional examination of these two elements is made in panel (b) of Figure 8 but now for the neutral species, [V I/Fe I] and [Ti I/Fe I]. There are fewer observational data available—nondetections and upper limits are not included—but the trends are similar, with most of the [Ti I/Fe I] ratios above solar and a strong correlation between the Ti and V abundance ratios. To get a sense of the observational limitations of the data and to

¹⁹ Note that the new atomic data for V I, V II, Co I, and Ni I that we applied to the spectrum of HD 84937 were not available for the Roederer et al. (2014) survey.

further examine the apparent correlation between these elements, we show in panel (c) of Figure 8 averages of [Ti I/Fe I] and [Ti II/Fe II] versus the average of [V I/Fe I] and [V II/Fe II]. This averaging process included 117 stars with all abundance states measured. This compares to more than 200 stars with just ionized-species abundances determined by Roederer et al. (2014). This figure panel shows much less scatter than seen in the individual plots: many of the “outlier” stars have vanished. Again, the average abundance ratios of almost all of the Ti data are above solar, while a number of the V values show greater variation. We again note that the plot includes only detectable species and does not include upper limits on V or Ti abundances in the data set of Roederer et al. (2014) which includes a total of more than 300 halo stars. The data of this figure panel confirm and strengthen the abundance correlation between V and Ti in low-metallicity stars.

We noted earlier that the Sc abundance was also above solar in HD 84937. In panel (d) of Figure 8 we examine the abundance ratios of [Sc/Fe] versus [Ti/Fe], both determined from their ionized species. While there is again scatter in the observational data, the same trends are seen in this plot as in the other three plots of the figure. Our new abundance ratios for [Sc/Fe] and [Ti/Fe] for HD 84937 are also consistent with the majority trend of other metal-poor halo stars.

In Figure 8 the Roederer et al. (2014) data show two stars that consistently exhibit very low Sc, Ti, and V abundances: BD+80 245 and CS 22169–035. These stars have been analyzed by other authors, and BD+80 245 was the first-discovered low-metallicity star with substantially subsolar α -element abundances (Carney et al. 1997). All authors who have studied these stars reach very similar conclusions on their Sc, Ti, and V abundances. Here we average results from neutral and ionized species of an element when both are available. For BD+80 245, Roederer et al. (2014) derived [Sc/Fe] = -0.40, [Ti/Fe] = -0.29, and [V/Fe] = -0.36. Carney et al. (1997) obtained [Ti/Fe] = -0.26 and did not analyze Sc and V. Ivans et al. (2003) derived [Sc/Fe] = -0.42, [Ti/Fe] = -0.30, and [V/Fe] = -0.39. For CS 22169–035 Roederer et al. (2014) found [Sc/Fe] = -0.40, [Ti/Fe] = -0.16, and [V/Fe] = -0.44. Giridhar et al. (2001) obtained somewhat larger abundance ratios, [Sc/Fe] = -0.13 and [Ti/Fe] = +0.06. However, two other studies are in accord with the Roederer et al. (2014) values: Honda et al. (2004) derived [Sc/Fe] = -0.33 and [Ti/Fe] = -0.13, while Cayrel et al. (2004) derived [Sc/Fe] = -0.18 and [Ti/Fe] = -0.07. We conclude that BD+80 245 and CS 22169–035 really are deficient in Sc, Ti, and V with respect to Fe. Their positions at the bottom of the V–Ti and Sc–Ti correlations are confirmed in multiple studies.

The observational data illustrated in the figures show that the three lightest Fe-group elements (Sc, Ti, and V) are correlated in metal-poor halo stars and thus appear to have closely related nucleosynthetic origins. In the future it will be important to make further precise abundance determinations in the metal-poor halo stars utilizing the new atomic laboratory data for the iron-peak elements.

The production of Ti and V in core-collapse supernovae (CCSNe) has been studied in detail (see, e.g., the discussion in Woosley & Weaver 1995, and references therein), and explosive stellar yields are available for different metallicities (e.g., Woosley & Weaver 1995; Limongi et al. 2000; Rauscher et al. 2002; Heger & Woosley 2010; Chieffi & Limongi 2013;

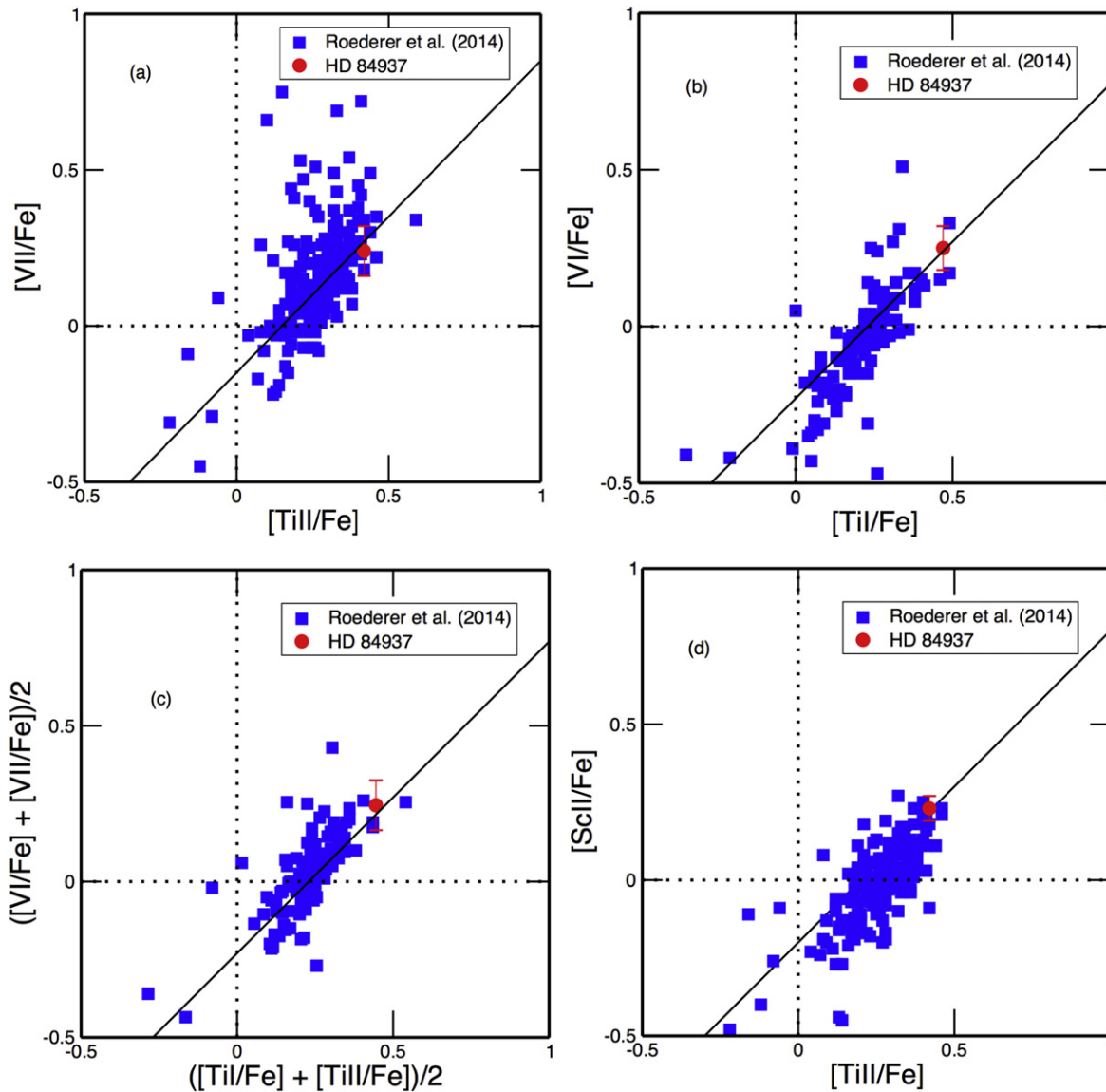


Figure 8. (a) Abundance ratios $[V/Fe]$ versus $[Ti/Fe]$ from ionized transitions of each element. The filled squares are from Roederer et al. (2014), and the filled circle for HD 84937 is derived in this paper. The horizontal and vertical (dotted) lines denote the solar abundance ratios of each element. The solid line represents a 45° slope. (b) Another V versus Ti correlation, this time from the neutral species of each element. (c) Means of $[Ti\ I/Fe\ I]$ and $[Ti\ II/Fe\ II]$ abundance ratios plotted versus means of $[V\ I/Fe\ I]$ and $[V\ II/Fe\ II]$ abundance ratios. (d) Abundance ratios $[Sc/Fe]$ versus $[Ti/Fe]$ from ionized transitions of each element.

Nomoto et al. 2013; Pignatari et al. 2013). In particular, ^{48}Ti and ^{49}Ti (which account for 73.7% and 5.4% of the solar Ti, respectively) are mostly made in the explosive Si-burning stellar layers, as ^{48}Cr and ^{49}Cr . Additionally, ^{46}Ti (8.2% of the solar Ti) is predominantly produced by explosive O burning. ^{47}Ti is primarily formed as itself by O burning and as ^{47}V in explosive Si burning, but in general it is underproduced by CCSNe compared to the previous Ti isotopes. Finally, ^{50}Ti is not efficiently made in baseline SN explosions. ^{51}V (99.75% of the solar V) is produced largely as ^{51}Mn in explosive Si-burning conditions and as ^{51}Cr in explosive O burning.

As an example, in Figure 10 we show the production of Ti and V in the ejecta of a $15 M_\odot$ ($Z = 0.01$) star CCSN (Pignatari et al. 2013). The presupernova stellar structure has been calculated with the stellar code GENEC (Eggenberger et al. 2008). The CCSN explosion simulations are based on the prescription by Fryer et al. (2012). These results confirm the nucleosynthesis scenario described above for baseline 1D

CCSN models. In particular, V is produced in explosive Si burning together with ^{48}Ti and ^{49}Ti , and in explosive O burning with ^{46}Ti , with similar V/Ti ratios for the two components of the SN ejecta. From Figure 10, we also observe that the conditions yielding the most efficient production of ^{56}Ni at mass coordinate $M \sim 2 M_\odot$ is V- and Ti-poor. Therefore, it is possible to have Fe production that is semidetached from V and Ti production in deep ejecta of baseline CCSN models, while synthesis of V and Ti are more coupled in the same fusion conditions. Within this scenario, the elemental ratio V/Ti observed in metal-poor stars can be used to explore the properties of explosive Si-burning and O-burning regions. The observed correlation of V and Ti may be a signature of this common production. This makes clear how important it is to have consistent observations with small errors and reliable atomic physics employed for a large sample of stars. In principle, the theoretical elemental ratios from stellar models could be compared with observations to directly constrain

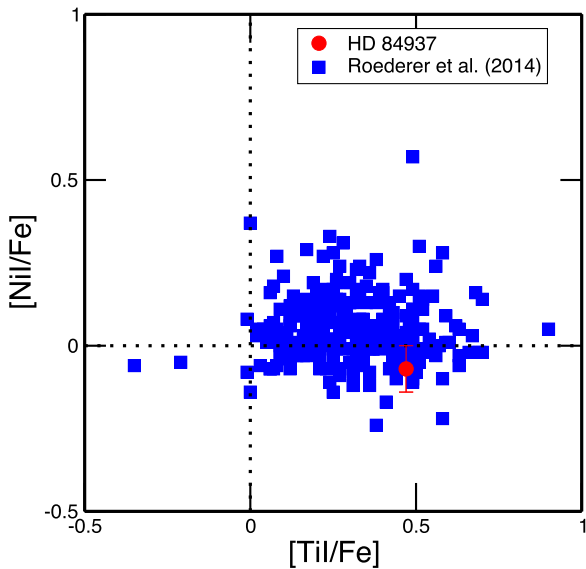


Figure 9. Abundance ratios $[\text{Ni}/\text{Fe}]$ versus $[\text{Ti}/\text{Fe}]$ from neutral transitions of each element. The symbols and lines are as in Figure 8.

specific regions of the CCSN ejecta where Ti and V are produced. The real stellar abundance scatter, above any observational errors, would also provide crucial information about different nucleosynthetic components hiding in these old stars. This work started with HD 84937 is an important step in this direction that needs to be extended to other stars in the future.

In panel (d) of Figure 8 we have seen that Sc production seems also to be correlated with Ti in the observational data. Such a correlation is not obvious from the theoretical point of view. Sc can be synthesized in the same astrophysical site as Ti, but it has a more complex production history. The monoisotopic Sc can be made as radiogenic ^{45}Ti in explosive O-burning and Si-burning layers together with Ti and V (Woosley & Weaver 1995). However, Sc can be also produced more efficiently as a result of neutrino feedback (e.g., Woosley & Weaver, Fröhlich et al. 2006a) or in α -rich freeze-out conditions. We will return to a discussion of Sc in Section 5. Nevertheless, it is clear that with all these different possible components the ratios Sc/Ti and Sc/V potentially are a less direct constraint than the Ti/V ratio. Interestingly, despite all these different nucleosynthesis paths to make Sc, theoretical stellar yields of CCSNe severely underestimate the observed Sc abundances compared to Fe in the early Galaxy (see also the next section).

In addition to V and Sc, we also examined other possible correlations of iron-peak elemental abundances with those of Ti. Specifically, we employed the Ni I abundance data from Roederer et al. (2014), and in Figure 9 we have plotted their $[\text{Ni I}/\text{Fe}]$ ratios as a function of $[\text{Ti I}/\text{H}]$. Inspection of this figure reveals a scatter plot with no obvious correlations. The $[\text{Ni I}/\text{Fe}]$ value of HD 84937 is unremarkable in this figure. We also note the two very low-abundance Ti stars (BD+80 245 and CS 22169–035) at the far left of Figure 9. As noted above, these stars are deficient in Ti, Sc, and V with respect to iron, but their Ni abundances do not show a similar low abundance trend and are consistent with that of HD 84937. This lends further support to the idea that Ni is synthesized in a different process or environment than are the elements Sc, Ti, and V. We made a

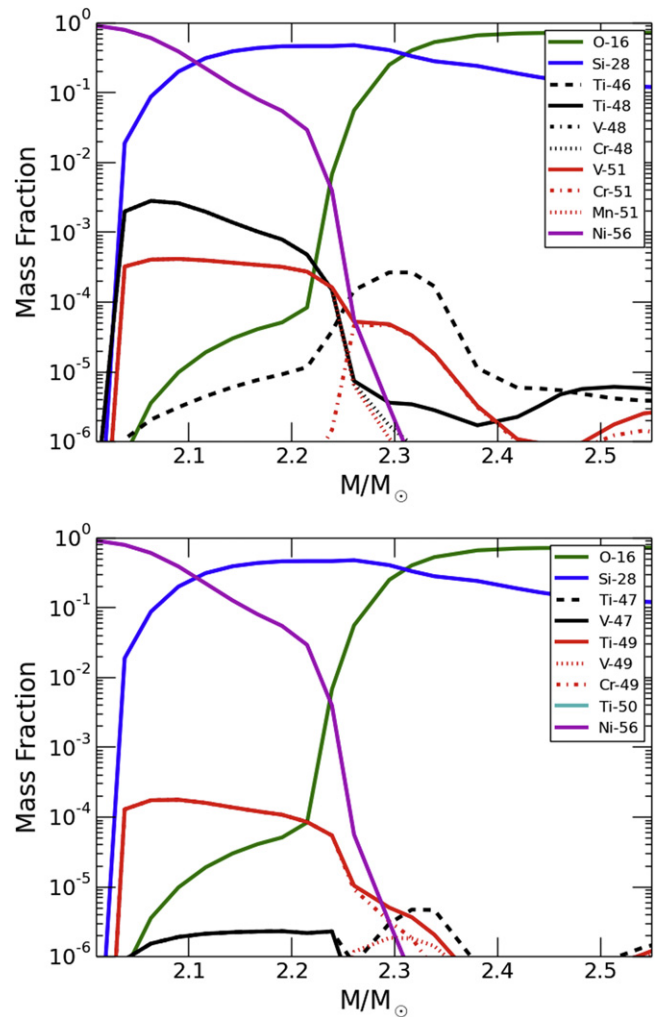


Figure 10. Upper panel: isotopic abundances in the explosive Si-burning and O-burning ejecta of the $15M_{\odot}$ SN model (Pignatari et al. 2013). Shown are profiles for ^{16}O , ^{28}Si , ^{46}Ti , ^{48}Ti , and its radiogenic parent isotopes ^{48}V and ^{48}Cr , ^{51}V and its radiogenic parent isotopes ^{51}Cr and ^{51}Mn , and ^{56}Ni . The unstable isotope ^{56}Ni will decay to ^{56}Co and finally to ^{56}Fe , which is most of the Fe SN ejecta. Lower panel: the same of the upper panel, but for ^{47}Ti and its radiogenic parent isotope ^{47}V , ^{49}Ti and its radiogenic parent isotopes ^{49}V and ^{49}Cr , and for ^{50}Ti .

similar analysis (with Ti) for the element Mn and found a similar result—no correlation between abundances derived from Mn I and Ti I. Thus, among the iron-peak elements, only Sc and V appear to be correlated with Ti production.

As a further comparison, we examined the α -group element Mg in the Roederer et al. (2014) data. The α elements are thought to be produced mainly in massive stars. Sneden et al. (2008) compiled $[\text{Mg}/\text{Fe}]$ data published in surveys to that date, showing that this abundance ratio shows very little star-to-star scatter at all metallicities, even for $[\text{Fe}/\text{H}] < -3$, and that at early times in the Galaxy, both Fe and Mg were being synthesized in the same types of stars. An analysis of Mg I with Ti I from Roederer et al. (2014) shows no such behavior and only a scatter plot.

5. IMPLICATIONS FOR EARLY GALACTIC NUCLEOSYNTHESIS

For solar-neighborhood stars with metallicities of $[\text{Fe}/\text{H}] \lesssim -1$, the Fe-group elements were predominantly

made by CCSNe. In these early stages, thermonuclear supernovae (Type Ia supernovae, SNe Ia; Hillebrandt et al. 2013 and references therein) did not have time to efficiently contribute to the galactic chemical inventory (Matteucci & Greggio 1986; Kobayashi & Nomoto 2009). Therefore, by comparing the observations of Fe-group elements in HD 84937 and other metal-poor stars with GCE models, it is possible to provide direct constraints on CCSN predictions. In particular, these elements are ideal sources of information about the details of SNe explosions. While light elements like O and Mg are mostly made in the pre-SN stage, Fe-group elements are mostly made during the explosion in the deepest part of the ejecta (e.g., Nomoto et al. 2013, for a review). Although there has been great progress in multidimensional simulations of SN explosions in recent years, the CCSN engine (Hix et al. 2014, and references therein) and subsequent propagation of the SN shock through the progenitor structure (Wongwathanarat et al. 2015) are uncertain at present. Modern CCSN yield sets are still calculated with 1D codes (e.g., Nomoto et al. 2013), and multidimensional effects have not been included in the GCE models yet.

During a supernova explosion, the elements that are synthesized in different stellar layers should mix to some extent, and some fraction of this mixed material will fall back onto the remnant (a neutron star or a black hole). Recent nucleosynthesis yields have been calculated with this fallback (i.e., mass cut; Kobayashi et al. 2006; Heger & Woosley 2010; Limongi & Chieffi 2012) and mixing (Kobayashi et al.). In this last paper’s yields, the ejected iron masses are constrained with independent parameters, i.e., the observed light curves and spectra of nearby supernovae (Nomoto et al. 2013). Hypernovae (with stellar masses of $M \geq 25M_{\odot}$) have explosion energies 10 times higher than normal SNe. In our GCE models, we assume a 50% hypernovae fraction, as did Kobayashi et al.

In CCSN ejecta, Cr and Mn are synthesized in the incomplete-Si-burning regions, while Co, Ni, Cu, and Zn are synthesized in the more central, complete-Si-burning regions. Therefore, $[(\text{Cr}, \text{Mn})/\text{Fe}]$ and $[(\text{Co}, \text{Ni}, \text{Cu}, \text{Zn})/\text{Fe}]$ ratios depend on the mixing-fallback parameters. On the other hand, the ratios among them, e.g., $[\text{Mn}/\text{Cr}]$, are more sensitive to the number of electrons per nucleon, Y_e (see Section 3.3 of Nomoto et al. 2013 for the details). Despite these complicated parameter dependencies, the GCE models are in good agreement with observations except for Sc, Ti, and V (Kobayashi et al. 2006, 2011b).

In GCE models, the contributions from various supernovae with different masses, metallicities, and energies are integrated according to the star-formation history of the system considered. In this paper, we use three GCE models for the solar neighborhood: Kobayashi et al. (2006, 2011b) and a new model (hereafter called the 2015 model) that includes a jet effect with the 2011 model. In reality, hypernovae should be jet-like explosions, and Maeda & Nomoto (2003) showed that some Fe-peak elements are significantly enhanced by the strong α -rich freeze-out due to high temperatures and high entropies in complete Si burning with bipolar models. However, nucleosynthesis yields with such 2D models have been calculated only for a small number of parameter sets. Therefore, we estimate a typical enhancement from the yields in Tominaga 2009 ($40M_{\odot}$, $Z = 0$, model C) and apply constant factors, +1.0, 0.45, 0.3, 0.2, and 0.2 dex for $[(\text{Sc}, \text{Ti}, \text{V}, \text{Co},$

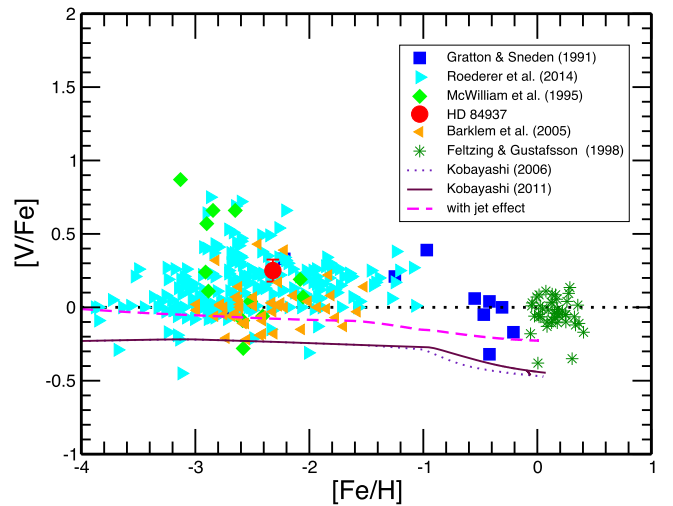


Figure 11. Abundance ratios $[V/Fe]$ plotted as functions of $[Fe/H]$ metallicity from Gratton & Sneden (1991), Roederer et al. (2014), McWilliam et al. (1995), Barklem et al. (2005), and Feltzing & Gustafsson (1998). The symbols are defined in the figure legend. The solid circle is the abundance value for HD 84937 derived in this paper. Overlaid on the figure are GCE models from Kobayashi et al. (2006; 2011; and this paper). See the text for detailed discussion.

and Zn)/Fe], respectively, to the hypernova yields with other parameters. Similar effects are expected also for 3D models that naturally show a large inhomogeneity (e.g., Janka 2012; Bruenn et al. 2013; Burrows 2013), although the nucleosynthesis yields are not available yet.

All GCE models assume an infall of primordial gas from outside the disk region, star formation proportional to the gas fraction, and no outflow. The model parameters are determined to meet the observed metallicity distribution function. The Salpeter (1955) initial mass function (IMF) and Kroupa (2001) IMF are adopted for the 2006 and 2011/2015 models, respectively. Note that the contributions from asymptotic giant branch (AGB) stars are also included in the 2011/2015 models, but the elemental abundances of Fe-peak elements are not affected at all. In all models, the contributions from SNe Ia are included as Chandrasekhar-mass explosions from single degenerate systems (Kobayashi et al. 1998; Kobayashi & Nomoto 2009; see, e.g., Kobayashi et al. 2015 for other progenitor models). The delay-time distributions of SNe Ia are slightly different between the 2006 and 2011 models. The nucleosynthesis yields of a deflagration are adopted in the 2006/2011 models, while those of a delayed detonation (Seitenzahl et al. 2013a, the N100 model) are adopted in the 2015 model.

To illustrate these GCE trends of the iron-peak elements, particularly at low metallicities, we first focus in detail on the $[V/Fe]$ abundance ratios as a function of $[Fe/H]$ in Figure 11. The observational data span decades and include large-sample surveys such as Gratton & Sneden (1991), McWilliam et al. (1995), Feltzing & Gustafsson (1998), Barklem et al. (2005), and Roederer et al. (2014). We again note that these earlier observations did not have access to the most up-to-date laboratory data and had to rely on then-current literature values. Nevertheless, the overall trends are clear. First, most of the $[V/Fe]$ abundance values in these low-metallicity stars are above the solar value: note the dashed horizontal line in Figure 11. The data also show a rise at low metallicities; our

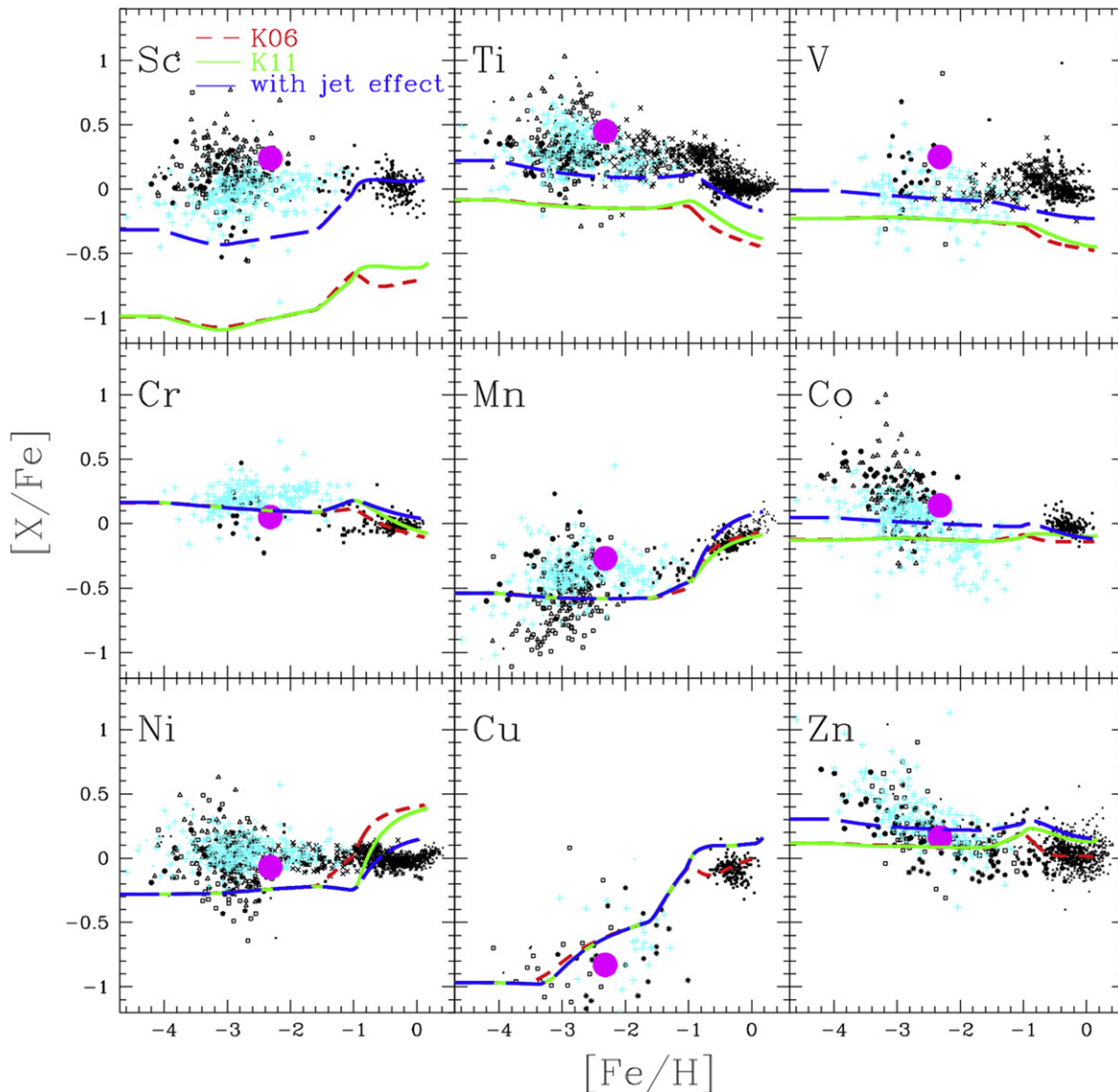


Figure 12. Abundance ratios of iron-peak elements plotted as functions of $[\text{Fe}/\text{H}]$ metallicity from a number of observational studies (see text for discussion). The solid magenta circles represent the HD 84937 abundance ratios derived in this paper. Overlaid on the figure are GCE models from Kobayashi et al. (2006, 2011b) and this paper. See the text for detailed discussion.

new value of $[\text{V}/\text{Fe}]$ for HD 84937 is consistent with that trend. We also note the large scatter in abundance values for these stars at lower metallicities. Superimposed on these data are several GCE model curves. These include Kobayashi et al. (2006, 2011b) and the new model with the jet effects, indicated by the dashed line in Figure 11. It is seen in the figure that including additional physics effects has led to increasing agreement between theory and observations.

Figure 12 gives an overview of the evolution of all Fe-peak elements in the solar neighborhood. The large filled circles are the mean abundances of HD 84937 from Table 5. The black dots represent observational data before 2014 (Fulbright 2000; Primas et al. 2000; Gratton et al. 2003; Reddy et al. 2003; Cayrel et al. 2004; Honda et al. 2004; Feltzing et al. 2007; Nissen et al. 2007; Saito et al. 2009; Cohen et al. 2013; Yong et al. 2013), and the cyan plus signs are from Roederer et al. (2014). Elements Sc, Ti, V, and Cr have some abundance information from both neutral and ionized species in various literature sources. In Figure 12 we have chosen to plot only

abundances derived from Sc II, Ti I, V I, and Cr II. For Ti, V, Cr, Ni, Cu, and Zn there is excellent accord between the survey results of Roederer et al. (2014) and those of the other included literature studies, but systematic offsets of $\sim 0.2\text{--}0.3$ dex are apparent for Sc, Mn, and Co. The reasons for these shifts deserve systematic investigation in future studies.

The difference in the adopted IMFs is negligible, and the 2006 (red short-dashed lines) and 2011 (green solid lines) models give almost the same trends at $[\text{Fe}/\text{H}] \lesssim -1$. The small difference at $[\text{Fe}/\text{H}] \gtrsim -1$ between the 2006 and 2011 models is caused by the small difference in the delay-time distributions of SNe Ia. The blue dashed lines of Figure 12 include the effects of jet-like explosions of hypernovae, and one sees that these models are much closer to the observational data, especially for Sc, Ti, V, and perhaps Zn. In addition, the ν -process also enhances Sc, V, and Ti isotopes $^{46,47,49,50}\text{Ti}$ in the yields calculated in Kobayashi et al. (2011a). We note that currently the new GCE model illustrated in Figures 11 and 12 underproduces the observed Sc, V, and Ti abundance ratios in

HD 84937 and in the bulk of stars. Nevertheless, the interplay between the multidimensional effects and additional neutrino effects (e.g., the ν -processes), may increase the predicted production of Sc, Ti, and V abundances, making them closer to those that are observed.

Detailed explorations of models and abundances for all Fe-group elements are beyond the scope of this paper, but a few other comments here are appropriate. Cr abundances are consistent with all these models, which has been shown in the comparison with the Cr II observations in Kobayashi et al. (2006). $[\text{Mn}/\text{Fe}]$ seems ~ 0.1 – 0.2 dex lower in the models than in the observations at $[\text{Fe}/\text{H}] \lesssim -1$, which can be easily solved with varying Y_e . Both in the observations and GCE models, the $[\text{Mn}/\text{Fe}]$ ratio shows an increasing trend from $[\text{Fe}/\text{H}] \sim -1$ to ~ 0 because Mn is produced more by SNe Ia than by core-collapse supernovae. This Mn increase cannot be reproduced with other SN Ia models, such as double-degenerate systems or double detonations (Seitenzahl et al. 2013b; Kobayashi et al. 2015). $[\text{Ni}/\text{Fe}]$ seems ~ 0.3 dex lower in the models than in the observations at $[\text{Fe}/\text{H}] \lesssim -1$, which may be difficult to solve because Ni and Zn have an opposite response to Y_e . Ni is overproduced by SNe Ia in the short-dashed and solid lines at $[\text{Fe}/\text{H}] \gtrsim -1$. As noted in Kobayashi et al. (2006), with delayed detonations, this Ni overproduction problem can be eased, which is included in the 2015 model (long-dashed lines). At $[\text{Fe}/\text{H}] \lesssim -2.5$, the observed $[\text{Co}/\text{Fe}]$ and $[\text{Zn}/\text{Fe}]$ ratios show a rising trend at lower metallicities. The observed Cu abundances are roughly consistent with the models. As demonstrated by Umeda & Nomoto (2002) and Kobayashi et al. (2006), higher explosion energies lead to higher values of $[(\text{Co}, \text{Zn})/\text{Fe}]$, so an even higher hypernovae fraction may be required at low metallicities.

6. SUMMARY AND CONCLUSIONS

We have conducted an extensive Fe-group elemental abundance analysis in the metal-poor main-sequence turnoff star HD 84937, involving nearly 1200 lines of 17 species. Derived abundances of neutrals and ions are the same within mutual uncertainties for all seven Fe-group elements with two species available for study. This strongly suggests that the standard Saha ionization balance holds for HD 84937 and that the observed abundance ratios among Fe-group elements can be treated as true measures of prior nucleosynthesis events.

The ~ 0.3 dex overabundances of Sc, Ti, and V relative to Fe in HD 84937 are of greatest nucleosynthetic interest. An examination of the abundances of Sc, Ti, and V suggest a correlation of their abundance enrichments in the early Galaxy. This may be due to a common nucleosynthesis origin for Ti and V in the CCSN ejecta, while the production of Sc is more complex. A more detailed analysis to clearly identify what components are dominating the production of Sc is needed.

GCE models cannot yet reproduce all of the observed abundance trends as a function of $[\text{Fe}/\text{H}]$ for these iron-peak elements, particularly at low metallicities. We explore the impact of new stellar models, and we discuss how observations can be used to constrain theoretical models of CCSNe and hypernovae. For HD 84937 we have derived $[(\text{Sc}, \text{Ti}, \text{V}/\text{Fe})] \simeq +0.3$, well above the observed uncertainties of $\lesssim 0.1$ dex from the species σ values. In the future, additional precise abundance determinations in metal-poor halo stars, taking advantage of new atomic laboratory data for the Fe-peak elements, should be undertaken. The results of this paper

suggest that with the additional inclusion of physics effects, the observational and theoretical agreement will improve.

We thank Tim Beers, John Norris, Craig Wheeler, Ian Roederer, and David Yong for helpful discussions about this work. Our referee and Pat Scott made very useful comments on the submitted manuscript, which led to improvement in the paper. This work has been supported in part by NASA grant NNX10AN93G (J.E.L.), by NSF grant AST-1211055 (J.E.L.), and by NSF grant AST-1211585 (C.S.). J.J.C. was supported in part by the JINA Center for the Evolution of the Elements, supported by the National Science Foundation under Grant No. PHY-1430152. M.P. acknowledges significant support to NuGrid from NSF grants PHY 09-22648 (Joint Institute for Nuclear Astrophysics, JINA), NSF grant PHY-1430152 (JINA Center for the Evolution of the Elements), and EU MIRGCT-2006-046520. M.P. acknowledges the support from the “Lendlet-2014” Programme of the Hungarian Academy of Sciences (Hungary) and from SNF (Switzerland).

REFERENCES

- Arcones, A., & Montes, F. 2011, *ApJ*, 731, 5
- Arsenen, A., Hallin, R., Nordling, C., et al. 1982, *A&A*, 106, 327
- Asplund, M., Grevesse, N., Sauval, A. J., & Scott, P. 2009, *ARA&A*, 47, 481
- Bard, A., Kock, A., & Kock, M. 1991, *A&A*, 248, 315
- Bard, A., & Kock, M. 1994, *A&A*, 282, 1014
- Barklem, P. S., Christlieb, N., Beers, T. C., et al. 2005, *A&A*, 439, 129
- Bergemann, M., & Gehren, T. 2008, *A&A*, 492, 823
- Bergeson, S. D., Mullman, K. L., Wickliffe, W. E., et al. 1996, *ApJ*, 464, 1044
- Blackwell, D. E., Lynas-Gray, A. E., & Smith, G. 1995, *A&A*, 296, 217
- Braut, J. W. 1976, *JOSA*, 66, 1081
- Brooke, J. S. A., Bernath, P. F., Schmidt, T. W., & Bacskay, G. B. 2013, *JQSRT*, 124, 11
- Brooke, J. S. A., Ram, R. S., Western, C. M., et al. 2014, *ApJS*, 210, 23
- Bruenn, S. W., Mezzacappa, A., Hix, W. R., et al. 2013, *ApJL*, 767, L6
- Burrows, A. 2013, *RvMP*, 85, 245
- Carney, B. W., Wright, J. S., Sneden, C., et al. 1997, *AJ*, 114, 363
- Cayrel, R., Depagne, E., Spite, M., et al. 2004, *A&A*, 416, 1117
- Chieffi, A., & Limongi, M. 2013, *ApJ*, 764, 21
- Cohen, J. G., Christlieb, N., McWilliam, A., et al. 2004, *ApJ*, 612, 1107
- Cohen, J. G., Christlieb, N., Thompson, I., et al. 2013, *ApJ*, 778, 56
- Cowan, J. J., & Rose, W. K. 1977, *ApJ*, 212, 149
- Delbouille, L., Roland, G., & Neven, L. 1973, Atlas photometrique du spectre solaire de $[\lambda] 3000$ a $[\lambda] 10000$ (Liege: Universite de Liege, Institut d’Astrophysique)
- Den Hartog, E. A., Lawler, J. E., Sobek, J. S., Sneden, C., & Cowan, J. J. 2011, *ApJS*, 194, 35
- Den Hartog, E. A., Ruffoni, M. P., Lawler, J. E., et al. 2014, *ApJS*, 215, 23
- Donnelly, M. P., & Hibbert, A. 2001, *MNRAS*, 321, 247
- Eggenberger, P., Meynet, G., Maeder, A., et al. 2008, *Ap&SS*, 316, 43
- Engström, L., Lundberg, H., Nilsson, H., Hartman, H., & Bäckström, E. 2014, *A&A*, 570, A34
- Farouqi, K., Kratz, K.-L., Pfeiffer, B., et al. 2010, *ApJ*, 712, 1359
- Fedchak, J. A., & Lawler, J. E. 1999, *ApJ*, 523, 734
- Feltzing, S., Fohlman, M., & Bensby, T. 2007, *A&A*, 467, 665
- Feltzing, S., & Gustafsson, B. 1998, *A&AS*, 129, 237
- Fröhlich, C., Hauser, P., Liebendörfer, M., et al. 2006a, *ApJ*, 637, 415
- Fröhlich, C., Martínez-Pinedo, G., Liebendörfer, M., et al. 2006b, *PhRvL*, 96, 142502
- Fryer, C. L., Belczynski, K., Wiktorowicz, G., et al. 2012, *ApJ*, 749, 91
- Fuhr, J. R., & Wiese, W. L. 2006, *JPCRD*, 35, 1669
- Fulbright, J. P. 2000, *AJ*, 120, 1841
- GharibNezhad, E., Shayesteh, A., & Bernath, P. F. 2013, *MNRAS*, 432, 2043
- Giridhar, S., Lambert, D. L., Gonzalez, G., & Pandey, G. 2001, *PASP*, 113, 519
- Gratton, R. G., Carretta, E., Claudi, R., Lucatello, S., & Barbieri, M. 2003, *A&A*, 404, 187
- Gratton, R. G., & Sneden, C. 1991, *A&A*, 241, 501
- Grevesse, N., Scott, P., Asplund, M., & Sauval, A. J. 2015, *A&A*, 573, A27
- Gurell, J., Nilsson, H., Engström, L., et al. 2010, *A&A*, 511, A68
- Heger, A., & Woosley, S. E. 2010, *ApJ*, 724, 341

- Herwig, F., Pignatari, M., Woodward, P. R., et al. 2011, *ApJ*, **727**, 89
- Hillebrandt, W., Kromer, M., Röpke, F. K., & Ruiter, A. J. 2013, *FrPhy*, **8**, 116
- Hinkle, K. H., Wallace, L., Ram, R. S., et al. 2013, *ApJS*, **207**, 26
- Hix, W. R., Lentz, E. J., Endeve, E., et al. 2014, *AIPA*, **4**, 041013
- Holweger, H., & Müller, E. A. 1974, *SoPh*, **39**, 19
- Honda, S., Aoki, W., Kajino, T., et al. 2004, *ApJ*, **607**, 474
- Ivans, I. I., Sneden, C., James, C. R., et al. 2003, *ApJ*, **592**, 906
- Janka, H.-T. 2012, *ARNPS*, **62**, 407
- Käppeler, F., Gallino, R., Bisterzo, S., & Aoki, W. 2011, *RvMP*, **83**, 157
- Kobayashi, C., Izutani, N., Karakas, A. I., et al. 2011a, *ApJL*, **739**, L57
- Kobayashi, C., Karakas, A. I., & Umeda, H. 2011b, *MNRAS*, **414**, 3231
- Kobayashi, C., & Nomoto, K. 2009, *ApJ*, **707**, 1466
- Kobayashi, C., Nomoto, K., & Hachisu, I. 2015, *ApJL*, **804**, L24
- Kobayashi, C., Tsujimoto, T., Nomoto, K., Hachisu, I., & Kato, M. 1998, *ApJL*, **503**, L155
- Kobayashi, C., Umeda, H., Nomoto, K., Tominaga, N., & Ohkubo, T. 2006, *ApJ*, **653**, 1145
- Kroupa, P. 2001, *MNRAS*, **322**, 231
- Kurucz, R. L. 2011, *CaJPh*, **89**, 417
- Lawler, J. E., Bonvallet, G., & Sneden, C. 2001, *ApJ*, **556**, 452
- Lawler, J. E., & Dakin, J. T. 1989, *JOSAB*, **6**, 1457
- Lawler, J. E., Guzman, A., Wood, M. P., Sneden, C., & Cowan, J. J. 2013, *ApJS*, **205**, 11
- Lawler, J. E., Sneden, C., & Cowan, J. J. 2015, *ApJS*, **220**, 13
- Lawler, J. E., Sneden, C., Cowan, J. J., Ivans, I. I., & Den Hartog, E. A. 2009, *ApJS*, **182**, 51
- Lawler, J. E., Wood, M. P., Den Hartog, E. A., et al. 2014, *ApJS*, **215**, 20
- Limongi, M., & Chieffi, A. 2012, *ApJS*, **199**, 38
- Limongi, M., Straniero, O., & Chieffi, A. 2000, *ApJS*, **129**, 625
- Lind, K., Bergemann, M., & Asplund, M. 2012, *MNRAS*, **427**, 50
- Lind, K., Melendez, J., Asplund, M., Collet, R., & Magic, Z. 2013, *A&A*, **554**, A96
- Lodders, K., Palme, H., & Gail, H.-P. 2009, *LanB*, **4**, 712
- Luck, R. E., & Bond, H. E. 1985, *ApJ*, **292**, 559
- Maeda, K., & Nomoto, K. 2003, *ApJ*, **598**, 1163
- Mansour, N. B., Dinneen, T., Young, L., & Cheng, K. T. 1989a, *PhRvA*, **39**, 5762
- Mansour, N. B., Dinneen, T. P., & Young, L. 1989b, *NIMPB*, **40**, 252
- Masseron, T., Plez, B., Van Eck, S., et al. 2014, *A&A*, **571**, A47
- Matteucci, F., & Greggio, L. 1986, *A&A*, **154**, 279
- McWilliam, A., Preston, G. W., Sneden, C., & Searle, L. 1995, *AJ*, **109**, 2757
- Meléndez, J., & Barbuy, B. 2009, *A&A*, **497**, 611
- Moore, C. E., Minnaert, M. G. J., & Houtgast, J. 1966, *The solar spectrum 2935 Å to 8770 Å* (National Bureau of Standards Monograph, Washington: US Government Printing Office (USGPO))
- Neuforge, C. 1993, in *Origin and Evolution of the Elements, A Revision of the Solar Abundance of Scandium*, ed. N. Prantzos, E. Vangioni-Flam, & M. Casse (Heidelberg: Astronomisches Rechen-Institut), 63
- Nilsson, H., Ljung, G., Lundberg, H., & Nielsen, K. E. 2006, *A&A*, **445**, 1165
- Nissen, P. E., Akerman, C., Asplund, M., et al. 2007, *A&A*, **469**, 319
- Nomoto, K., Kobayashi, C., & Tominaga, N. 2013, *ARA&A*, **51**, 457
- O'Brian, T. R., Wickliffe, M. E., Lawler, J. E., Whaling, W., & Brault, J. W. 1991, *JOSAB*, **8**, 1185
- Peterson, R. C., & Schrijver, C. J. 1997, *ApJL*, **480**, L47
- Pickering, J. C., Donnelly, M. P., Nilsson, H., Hibbert, A., & Johansson, S. 2002, *A&A*, **396**, 715
- Pickering, J. C., Johansson, S., & Smith, P. L. 2001, *A&A*, **377**, 361
- Pignatari, M., Gallino, R., Meynet, G., et al. 2008, *ApJL*, **687**, L95
- Pignatari, M., Herwig, F., Hirschi, R., et al. 2013, arXiv:1307.6961
- Primas, F., Brugamy, E., Sneden, C., et al. 2000, in *The Galactic Halo: From Globular Clusters to Field Stars*, Proc. 35th Liege International Astrophysics Colloquium, Copper and Zinc Abundances in Metal-poor Stars, ed. A. Noels, P. Magain, D. Caro et al. (Liege: Institut d'Astrophysique et de Geophysique), 119
- Raassen, A. J. J., & Uylings, P. H. M. 1998, *JPhB*, **31**, 3137
- Ram, R. S., Brooke, J. S. A., Bernath, P. F., Sneden, C., & Lucatello, S. 2014, *ApJS*, **211**, 5
- Rauscher, T., Heger, A., Hoffman, R. D., & Woosley, S. E. 2002, *ApJ*, **576**, 323
- Reddy, B. E., Tomkin, J., Lambert, D. L., & Allende Prieto, C. 2003, *MNRAS*, **340**, 304
- Roederer, I. U., Lawler, J. E., Sobeck, J. S., et al. 2012, *ApJS*, **203**, 27
- Roederer, I. U., Preston, G. W., Thompson, I. B., et al. 2014, *AJ*, **147**, 136
- Ruffoni, M. P., Den Hartog, E. A., Lawler, J. E., et al. 2014, *MNRAS*, **441**, 3127
- Saito, Y.-J., Takada-Hidai, M., Honda, S., & Takeda, Y. 2009, *PASJ*, **61**, 549
- Salpeter, E. E. 1955, *ApJ*, **121**, 161
- Schnabel, R., Schultz-Johanning, M., & Kock, M. 2004, *A&A*, **414**, 1169
- Scott, P., Asplund, M., Grevesse, N., Bergemann, M., & Sauval, A. J. 2015, *A&A*, **573**, A26
- Seitenzahl, I. R., Cescutti, G., Röpke, F. K., Ruiter, A. J., & Pakmor, R. 2013a, *A&A*, **559**, L5
- Seitenzahl, I. R., Ciaraldi-Schoolmann, F., Röpke, F. K., et al. 2013b, *MNRAS*, **429**, 1156
- Sikström, C. M., Schultz-Johanning, M., Kock, M., et al. 1999, *JPhB*, **32**, 5687
- Sneden, C. 1973, *ApJ*, **184**, 839
- Sneden, C., Cowan, J. J., & Gallino, R. 2008, *ARA&A*, **46**, 241
- Sneden, C., Lawler, J. E., Cowan, J. J., Ivans, I. I., & Den Hartog, E. A. 2009, *ApJS*, **182**, 80
- Sneden, C., Lucatello, S., Ram, R. S., Brooke, J. S. A., & Bernath, P. 2014, *ApJS*, **214**, 26
- Sobeck, J. S., Kraft, R. P., Sneden, C., et al. 2011, *AJ*, **141**, 175
- Sobeck, J. S., Lawler, J. E., & Sneden, C. 2007, *ApJ*, **667**, 1267
- Suda, T., Katsuta, Y., Yamada, S., et al. 2008, *PASJ*, **60**, 1159
- Thielemann, F.-K., Arcones, A., Käppeli, R., et al. 2011, *PrPNP*, **66**, 346
- Tominaga, N. 2009, *ApJ*, **690**, 526
- Travaglio, C., Gallino, R., Arnone, E., et al. 2004, *ApJ*, **601**, 864
- Umeda, H., & Nomoto, K. 2002, *ApJ*, **565**, 385
- Villemoes, P., van Leeuwen, R., Arnesen, A., et al. 1992, *PhRvA*, **45**, 6241
- Wallerstein, G., Greenstein, J. L., Parker, R., Helfer, H. L., & Aller, L. H. 1963, *ApJ*, **137**, 280
- Wallerstein, G., & Helfer, H. L. 1959, *ApJ*, **129**, 720
- Wanajo, S., Nomoto, K., Iwamoto, N., Ishimaru, Y., & Beers, T. C. 2006, *ApJ*, **636**, 842
- Wongwathanarat, A., Müller, E., & Janka, H.-T. 2015, *A&A*, **577**, A48
- Wood, M. P., Lawler, J. E., Den Hartog, E. A., Sneden, C., & Cowan, J. J. 2014a, *ApJS*, **214**, 18
- Wood, M. P., Lawler, J. E., Sneden, C., & Cowan, J. J. 2013, *ApJS*, **208**, 27
- Wood, M. P., Lawler, J. E., Sneden, C., & Cowan, J. J. 2014b, *ApJS*, **211**, 20
- Woosley, S. E., & Weaver, T. A. 1995, *ApJS*, **101**, 181
- Yong, D., Norris, J. E., Bessell, M. S., et al. 2013, *ApJ*, **762**, 26
- Young, L., Childs, W. J., Dinneen, T., et al. 1988, *PhRvA*, **37**, 4213